Development of a Lithium Hydride Powered Hydrogen Generator for Use in Long Life, Low Power PEM Fuel Cell Power Supplies

by

Daniel DeWitt Strawser

Bachelor of Science, Mechanical Engineering
Stanford University, 2010

Submitted to the Department of Mechanical Engineering
in Partial Fulfillment of the Requirements for the Degree of
Master of Science in Mechanical Engineering

at the

Massachusetts Institute of Technology

June 2012

Signature of Author: .....
Department of Mechanical Engineering
May 10, 2012

Certified by: .....
Steven Dubowsky
Professor of Mechanical Engineering
Thesis Supervisor

Accepted by: .....
David E. Hardt
Chairman, Department Committee on Graduate Theses

Development of a Lithium Hydride Powered Hydrogen Generator for Use in Long Life, Low Power PEM Fuel Cell Power Supplies

by

Daniel DeWitt Strawser

Submitted to the Department of Mechanical Engineering
on May 10, 2012 in Partial Fulfillment of the
Requirements for the Degree of Master of Science in
Mechanical Engineering

ABSTRACT

This thesis studies a hybrid PEM fuel cell system for use in low power, long life sensor networks. PEM fuel cells offer high efficiency and environmental friendliness but have not been widely adopted due to cost, reliability, and the problem of hydrogen storage. This thesis focuses on the problem of hydrogen storage. Lithium hydride is selected for study because of its high hydrogen content and because it produces hydrogen through a chemical reaction with water.

Control of the lithium hydride hydrolysis reaction is investigated. Active and passively-controlled hydrogen generators that rely on lithium hydride are designed and experimentally studied. A model is created to explain the system's pressure response. The passive hydrogen generator is experimentally tested in a 2 month benchtop fuel cell experiment.

The results of the study suggest that it is possible to design a simple, passive generator that controls the hydrogen pressure at an operating point. However, over longer time periods of 1-3 months, the rate of reaction slows significantly and byproduct formation prevents full utilization of the lithium hydride. These limits complicate the design of a power supply relying on lithium hydride.

TABLE OF CONTENTS

LIST OF FIGURES

LIST OF TABLES

CHAPTER

1

INTRODUCTION

This thesis investigates lithium hydride as a hydrogen source for use in low power, long life PEM fuel cell power systems. The investigation is carried out through the development and experimental study of a passively-controlled hydrogen generator.

Low power, long-life electronic devices such as sensor networks are becoming prevalent. The majority of these devices rely on batteries, which have limited lifetimes compared to the device's needs [1]. This thesis studies a hybrid PEM (Proton Exchange Membrane) fuel cell system for low power, long life applications. PEM fuel cells have high efficiency but have problems of cost, complexity, and the need for hydrogen storage . The focus of this thesis is on the hydrogen storage problem. Solid state hydrogen storage using lithium hydride is investigated. Lithium hydride is selected for study because of its high hydrogen content and because it only requires water to produce hydrogen gas, which the fuel cell then converts into electrical energy.

The research considers control of the lithium hydride hydrolysis reaction using both active and passive control. A model of a passively-controlled generator is produced and experimentally studied. The passively-controlled design is then experimentally studied in a 3 month benchtop fuel cell system. From the experimental results, lithium hydride is evaluated as a source of hydrogen for such low-power, long-life systems.

This research is conducted at the MIT Field and Space Robotics Laboratory (FSRL) under the guidance of Professor Steven Dubowsky. Considerable guidance was also provided by postdoctoral associate Jekanthan Thangavelautham.

1.1 Motivation

Low power sensor networks are becoming widespread. Example applications include environmental air-quality monitoring, reporting illegal border crossings in desert regions, and traffic sensors on busy highways [2]. In such sensor network applications, hundreds of thousands of sensors

are used over wide areas. These sensors are expected to last for years without maintenance or charging their battery. Although many advancements have been recently made involving the sensor modules, their power supplies are still lagging behind. State-of-the-art batteries will not meet the demand of many of these systems because they have low energy densities [3], [4]. This means that the best batteries will not be able to supply the years of operation required of these systems.

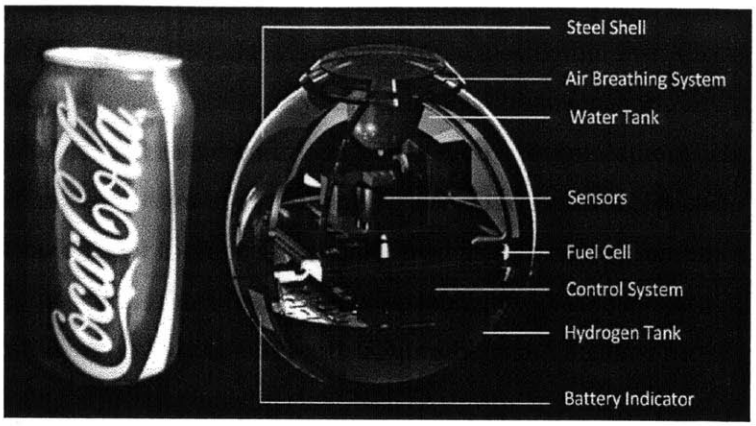

Figure 1: Example fuel cell sensor network module [57].

There must be a better solution. Fuel cells offer one potential solution because of their high energy density. A fuel cell is an electrochemical device that converts chemical energy to electrical energy. An example fuel cell sensor network module is presented in Figure 1.

Drawbacks of fuel cells include their reliability, complexity, and, in the case of PEM fuel cells, the need to store hydrogen fuel. However, recent research suggests that the reliability of fuel cells can be increased by controlling their operating conditions [5]. This thesis focuses on the problem of hydrogen storage in a PEM fuel cell, which is a non-trivial task . Conventional storage of hydrogen as a compressed gas or a liquid is bulky and not suitable for low-power applications. Research has been done on storage of hydrogen in metal hydrides and some hydrides have been brought to commercialization [6], [7]. Metal hydrides are compounds that contain a metal bonded to hydrogen. They produce hydrogen gas under various mechanisms including chemical reaction, pressure changes, and temperature changes. Metal hydrides are promising because of their large hydrogen weight efficiencies, their low overhead power requirements, and the simplicity with which certain hydrides release hydrogen.

Of the many metal hydrides available, this thesis investigates the potential of lithium hydride (LiH) for use in low power, long life fuel cell power systems. Lithium hydride has a high gravimetric hydrogen content; it is 12.5% hydrogen by weight, which is one of the highest of the metal hydrides. It produces hydrogen through a chemical reaction with water. A drawback of lithium hydride is that it cannot be easily regenerated [7]. This is unimportant for the applications

considered in this thesis because it is assumed the sensor modules would be recharged very infrequently.

Development of a hydrogen generator for use in low power, long life PEM fuel cell power systems presents a number of technical challenges. First, the design must be simple and reliable to operate for long periods of time. Second, the pressure of hydrogen must be controlled to maximize fuel cell performance, efficiency, and life. If the pressure is too low, the fuel cells will degrade due to a lack of hydrogen (hydrogen starvation), if the pressure is too high, hydrogen will be lost to the environment.

An effective hydrogen storage medium must be found. This thesis investigates if lithium hydride is suitable for use in low power, long life fuel cell systems. Chief concerns are whether lithium hydride can deliver the required rate of hydrogen and whether the hydrolysis reaction runs to 100% completion (i.e. whether the lithium hydride delivers the predicted amount of hydrogen). These factors are the principle engineering challenges discussed here.

In this thesis low power is defined as powers ranging from 10-250 mW and long life systems are those with lifespans of 3 months to 5 years.

1.2 System Concept

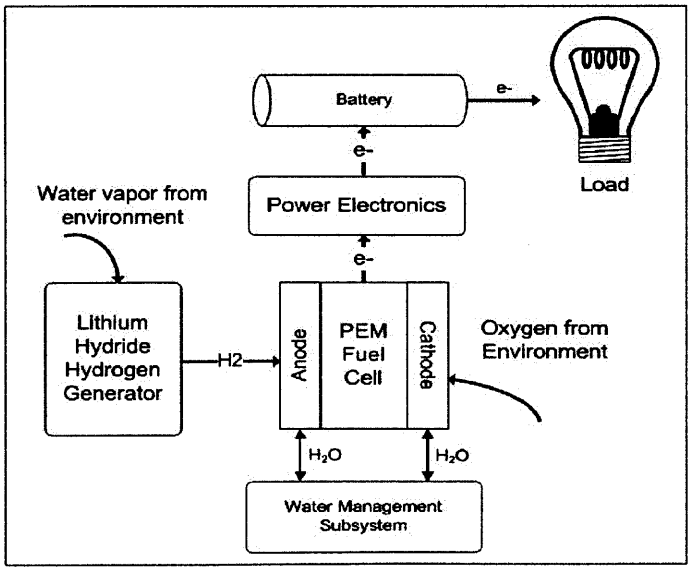

Figure 2: System concept for long-life, low-power PEM fuel cell system.

A concept for a hybrid low-power, long-life PEM fuel cell power system is shown in Figure 2. The PEM fuel cell uses oxygen from the environment and hydrogen produced by the

lithium hydride to generate electricity. The concept is termed a hybrid system because the fuel cell charges a battery, which then powers the sensor. This prevents the load's varying power demand from affecting the fuel cell, which can lead to degradation [8].

The focus of this research is on the lithium hydride hydrogen generator. The generator takes water vapor from the ambient environment, reacts the water vapor with lithium hydride, and generates hydrogen, which the fuel cell uses to produce power. It may be possible to activate the hydride using water produced at the fuel cell's cathode; however, this was not pursued in this research.

In addition to the hydrogen generator, other subsystems are necessary to maximize the fuel cell life. A water management subsystem ensures that the cathode remains at 30-70% relative humidity and that the anode remains at 100% relative humidity. Power electronics prevent voltage oscillations caused by the load to reach the fuel cells because this can degrade the fuel cell system [5].

1.3 PEM Fuel Cells

Proton Exchange Membrane (PEM) fuel cells are electrochemical devices that convert the chemical energy in hydrogen and oxygen into electricity. The basic workings of a PEM fuel cell are presented in Figure 3 [9]. Hydrogen enters at the anode where it reacts with a platinum catalyst. The hydrogen nucleus (a proton) travels across a polymer membrane to the cathode while its electron travels through an external circuit to generate electricity. At the cathode, the proton, electron, and an oxygen atom combine to form water. This means that PEM fuel cells can generate electricity while only exhausting water. The devices also have very high energy conversion efficiencies. Theoretical efficiencies come close to 83% and practical efficiencies are approximately 65% [10].

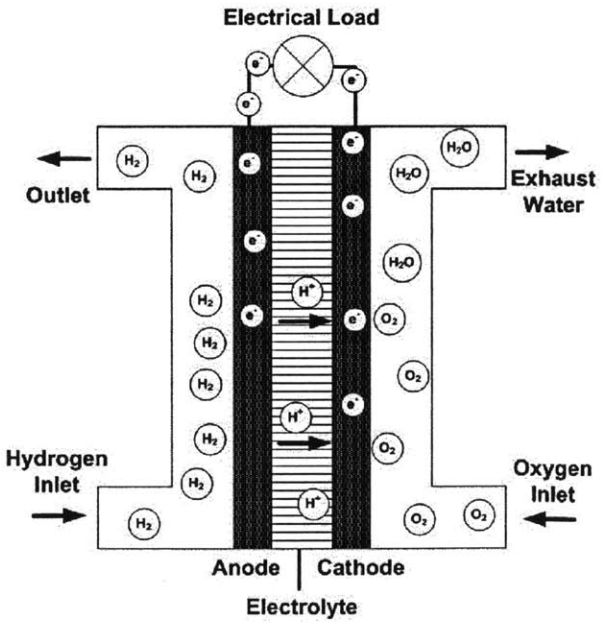

Figure 3: Schematic of PEM fuel cell. Adapted from a diagram in [9].

Although PEM fuel cells were invented in the 1960s, they are not widely used [11]. First, PEM fuel cells are expensive, mainly due to their need for a platinum catalyst to oxidize the hydrogen. Second, PEM fuel cells are subject to degradation. Thirdly, PEM fuel cells require storage of hydrogen, which is an engineering challenge.

1.4 Thesis Organization

The objective of this research is the development of a lithium hydride based hydrogen generator for low power, long life PEM fuel cell power systems. The potential of lithium hydride as a hydrogen source for low power, long life systems is evaluated.

Chapter 2 focuses on the selection of lithium hydride as a source of hydrogen. At the start of this research, lithium hydride was selected for three reasons: its high gravimetric hydrogen content, the simplicity with the reaction is controlled, and the assumption that the reaction reached 100% completion. The final assumption was incomplete, based on later experimental evidence.

Chapter 3 presents the design of a lithium hydride generator. Initially, active designs were attempted that pumped liquid water into the system or that relied on active valves. Finally, a passive design was pursued that relied on a compliant valve to regulate pressure.

Chapter 4 discusses the modeling work that was done on the generator's passive dynamics. The model was compared with experimental results.

Chapter 5 presents the benchtop prototype system that was used to study the passive generator in a fuel cell system. The experimental system was designed to run for 3 months and produce 250 mW average power. After 2 months, the fuel cells experienced hydrogen starvation and stopped producing power.

Chapter 6 focuses on research performed to explain why the prototype in Chapter 5 suffered hydrogen starvation. The experiments concentrated on the rate of hydrogen production over longer time periods (1-3 months) than previously considered and found that the rate significantly decreases.

Finally, Chapter 7 is not connected to the development of the hydrogen generator but presents work done during this thesis which investigates the problem of nitrogen building up in the anode while the fuel cell is operating in Dead Ended Anode (DEA) mode. A passive nitrogen release mechanism was developed.

CHAPTER

2

LITHIUM HYDRIDE AS A SOURCE OF HYDROGEN

Storage of hydrogen, the fuel of PEM fuel cells, is a difficult task [12]. This thesis focuses on storing hydrogen in lithium hydride, which is a type of metal hydride. A metal hydride is a compound of metal bonded with hydrogen. Lithium hydride releases hydrogen through chemical reaction with water to produce hydrogen gas and other byproducts. It was selected for this study because it has a high weight density of hydrogen, the production of hydrogen is simple to control by varying its exposure to water, and because it was assumed that lithium hydrogen is able to react almost completely.

2.1 Solid State Hydrogen Storage in Metal Hydrides

2.1.1 Hydrogen Economy

Hydrogen has long been advocated as a solution to the world's energy problems [13]. Hydrogen has the highest energy density of any substance in the universe with 286 kJ/mol. Additionally, it is the most abundant element in the universe and composes over 75% of all matter [14]. To convert hydrogen's chemical energy into electrical energy, it can be used in fuel cell devices, which offer high efficiencies and are environmentally friendly because they only exhaust water.

There are also many drawbacks. While hydrogen is the most abundant element in the universe, it rarely exists by itself on earth and must be extracted from other compounds. Approximately 95% of hydrogen used today comes from the steam reforming of natural gas, which makes hydrogen as neither as clean nor as efficient as it would otherwise be [15].

Two of the most common methods of storing hydrogen are compressing it to hundreds of megapascals or storing it as a liquid. Because of their complexity and high energy overhead,

neither of these methods were thought practical for this study. This research focuses on a class of hydrogen storage materials known as metal hydrides.

2.1.2 Metal Hydrides

Metal hydrides are a wide range of compounds that feature hydrogen bonded to a metal. Each hydride has different chemical characteristics including hydrogen weight content and hydrogen release mechanism. Figure 4 contains a graph of various hydrides and their percent weight of hydrogen [16].

2.1.3 Reversible vs. Nonreversible Hydrides

Metal hydrides are commonly classified based on how they release hydrogen. Reversible or pressure-release hydrides are hydrides that release hydrogen through changes in pressure. The second group is termed irreversible or chemical-release hydrides, which release hydrogen through chemical reaction. Pressure-release hydrides are classified as reversible because it normally requires much less energy to regenerate them than chemical-release hydrides. Many will reabsorb hydrogen simply by exposing them to hydrogen gas at a high pressure. Chemical-release hydrides require greater amounts of energy and it is often considered impractical to recharge them. On the other hand, chemical release hydrides normally have higher hydrogen

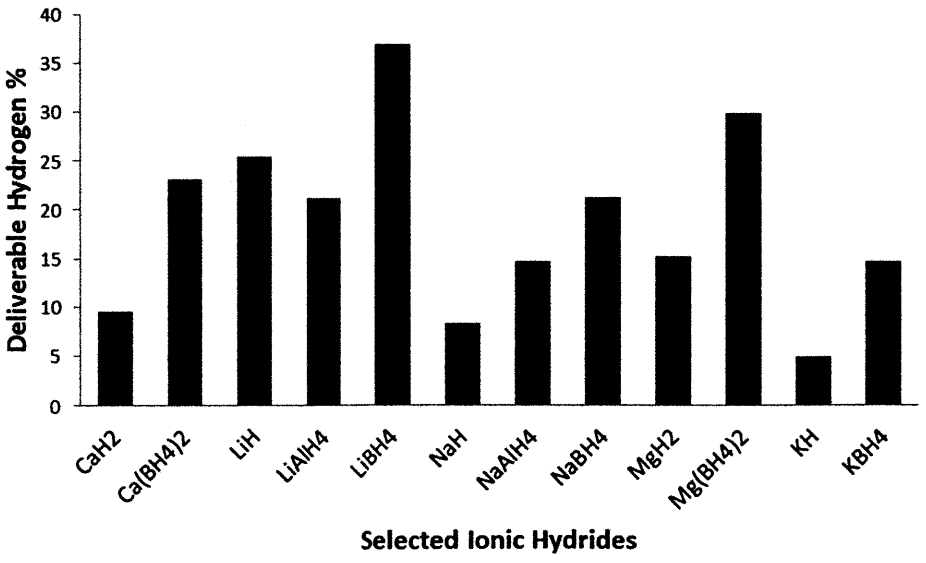

Figure 4: Maximum hydrogen weight efficiencies of various ionic hydride [16].

content than reversible hydrides. These classes are not mutually exclusive; under certain circumstances, reversible hydrides may release hydrogen through irreversible processes [16].

Currently, much research is being devoted to complex hydrides because of their high hydrogen content and potential to be recycled. However, many of these require external catalysts and have other constraints. For example, sodium borohydride, $NaBH_4$, promises high gravimetric content of hydrogen but requires a catalyst and must be mixed in a solution to prevent catalyst degradation [17].

2.2 Lithium Hydride

Of the various hydrides, lithium hydride (LiH) was chosen for study because it best met the research objectives outlined in the introduction for long life, low power systems. Before describing the suitability of lithium hydride for this project, the compound's chemistry is discussed. Despite being studied for almost 50 years [18], its chemistry is still not fully understood and competing theories exist as to what controls the release of hydrogen.

2.2.1 Background of Lithium Hydride

Lithium hydride has long been considered a potential source of hydrogen in PEM fuel cells. It served as the hydrogen source for the first PEM fuel cells developed by General Electric and the US Army in the 1960s [19], [11]. Since this original study, the compound has been often considered as a hydrogen storage mechanism for PEM fuel cells. Past research has investigated lithium hydride's potential for use in underwater vehicles [20] and for automobile transportation [21]. Lithium hydride is often bypassed as a source of hydrogen because of the high energy costs to regenerate [22]. The ability to regenerate the hydride is not important in this study because it is assumed that the sensor cannot be refueled once placed into operation.

In addition to energy storage, lithium hydride finds wide use as neutron shielding in nuclear reactors [23]. Lithium hydride's radioactive isotope, lithium deuteride, is used for fusion in hydrogen bombs [24].

A large amount of research has been devoted to the compound's chemistry and a comprehensive literature review is found in [25]. The chemistry relevant to this research will be discussed next.

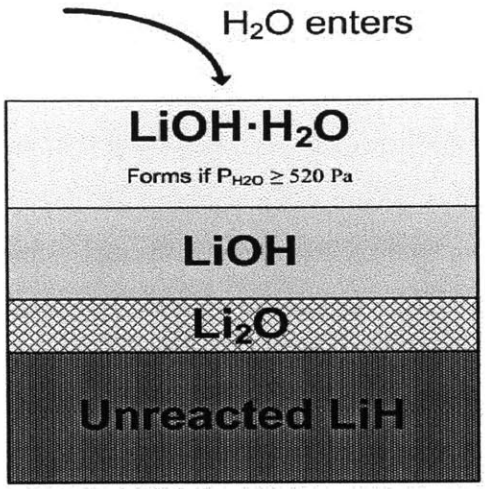

Figure 5: Layering of products of LiH hydrolysis reaction [25].

2.2.2 Hydrolysis of LiH

The reaction of interest to this study is the production of hydrogen from lithium hydride, which occurs when the compound reacts with water. This reaction is exothermic and releases 90.7 kJ/mol of hydride [26]. The chemical equation for this reaction is:

$$LiH + H_2O \rightarrow LiOH + H_2 \qquad (1)$$

Although (1) helps one understand the overall hydrogen-generating process, it is oversimplified. The true reaction occurs in a series of steps with products depending on temperature, hydrogen partial pressure, and water partial pressure (relative humidity) [27]. Lithium hydroxide (LiOH) or lithium hydroxide monohydrate ($LiOH \cdot H_2O$) are the favored byproducts under pressures and humidities considered in this study [25]. If the hydrolysis reaction is carried out in an air atmosphere containing carbon dioxide, lithium hydroxide will react with carbon dioxide to produce lithium carbonate (Li_2CO_3) [28].

The layers of byproducts that form on lithium hydride during hydrolysis are depicted in Figure 5. The product lithium hydroxide forms a thickening layer through which water must pass for the reaction to continue. Between the lithium hydride and hydroxide exists a thin layer of lithium oxide. This layer is only a few hundred Angstroms thick but must exist because

lithium hydride and lithium hydroxide cannot thermodynamically exist next to one another. This layer, which is believed to maintain constant thickness as the reaction proceeds, is important when considering the rate of reaction [29].

The formation of lithium hydroxide monohydrate ($LiOH \cdot H_2O$) is important to this study. Lithium hydroxide monohydrate occurs when water molecules bond to the lithium hydroxide crystal and forms when lithium hydroxide is exposed to relative humidities greater than 15% and temperatures less than 50° C [30]. Lithium hydroxide monohydrate releases its water when heated to above 100° C [31]. Because one mole of lithium hydroxide will absorb one mole of water, lithium hydroxide monohydrate formation has implications on generator design; specifically, more water is required than would be otherwise necessary.

Given the above product layers, a more complete description of the hydrolysis reaction is the following series of equations given in [32]:

$$2LiH + H_2O \rightarrow Li_2O + 2H_2 \tag{2}$$

$$Li_2O + H_2O \rightarrow 2LiOH \tag{3}$$

Given proper humidity conditions, the following will occur:

$$LiOH + H_2O \rightarrow LiOH \bullet H_2O \tag{4}$$

Depending on the presence of carbon dioxide, lithium carbonate will form:

$$2LiOH + CO_2 \rightarrow Li_2CO_3 + H_2O \tag{5}$$

These equations indicate that lithium hydride first produces hydrogen gas and lithium oxide. The lithium oxide then reacts with water to form lithium hydroxide (or lithium hydroxide monohydrate).

2.2.3 Rate of Hydrogen Production – Tri-layer Model

The controlling mechanism of the rate of hydrogen production has been well studied and debated in literature [25]. Early work found in [18] mentions that the rate of hydrogen production

is not controlled by diffusion of water vapor through the product layer of lithium hydroxide while work presented in [33] claims that diffusion has a substantial effect. The most recent theory supported by [34], [30], and [29] is the "trilayer model." A diagram of this model is shown in Figure 5. Instead of lithium hydride and lithium hydroxide existing next to one another (which is unstable chemically), a thin layer of lithium oxide (less than 100 Angstroms) forms between the lithium hydride and the lithium hydroxide. According to this model, micro-cracks develop in the lithium hydroxide layer as it forms. The micro-cracks are due to differences in the lattice structure between lithium hydride and lithium hydroxide. They allow water vapor to penetrate through to the unreacted hydride bed. Throughout the hydrolysis process, the layer of lithium oxide maintains constant thickness and it is the layer of lithium oxide, not lithium hydroxide, which is the rate-controlling mechanism [29].

This theory has important implications for this study because it means that the hydrolysis reaction should not "clog up" over time; water vapor should be able to reach the hydride through micro-cracks and hydrolysis should continue. This characteristic, if true over long periods of time, makes lithium hydride ideal for long-life, low power PEM fuel cell systems.

2.3 Suitability of LiH for PEM Fuel Cell Systems

Of the many forms of hydrogen storage, lithium hydride was selected for study for long-life, low-power systems because of three characteristics: its high hydrogen content, the simplicity with which the reaction is controlled, and the hypothesis that the reaction does not clog up over long periods of time.

2.3.1 High Gravimetric Weight Content of Hydrogen

The first reason lithium hydride was selected for study is its high gravimetric weight content of hydrogen. Table 1 shows lithium hydride compared with a variety of actively researched hydrides. Certain borohydrides have higher weight densities, but many, such as sodium borohydride, (NaBH4) require complex catalysts, which are prone to degradation [17]. Beryllium borohydride has a very high hydrogen content but is too reactive and toxic to be considered [35]. Alkali metal hydrides, such as calcium hydride, sodium hydride, and lithium hydride are all simpler in the sense that they only require water to produce hydrogen. Of these hydrides, lithium hydride has the highest hydrogen weight content.

That lithium hydride only requires water to produce hydrogen gives it an even higher weight efficiency. For the low powers considered in this thesis, water is available either from the environment (as water vapor) or from the fuel cell's exhaust. This means that water does not need to be carried with the system. For every gram of LiH in a power supply, 0.25 grams of hydrogen can theoretically be produced. This yields a weight efficiency of 25%.

Hydride	Gravimetric Hydrogen Weight Content
LiBH4	18.4%
NaBH4	10.6%
Be(BH2)4	20.8%
NaAlH4	7.4%
NaH	4.1%
CaH2	4.7%
LiH	12.5%

Table 1: Table of various hydrides and their gravimetric hydrogen content, defined as the mass of the hydrogen divided by the total mass of the hydride. Derived from information in [36].

2.3.2 Controlling Lithium Hydride Hydrolysis

The second reason for choosing lithium hydride is that the reaction is simple; hydrogen production only requires application of liquid water or water vapor. This indicates that in order to control the reaction, it is necessary to control the amount of water reaching the hydride.

A series of experiments conducted in this study show the hydrolysis reaction's dependence on the relative humidity of the atmosphere surrounding the hydride. The dependence of the rate of hydrogen production on exposed lithium hydride surface area is also investigated. These experiments use the setup depicted in Figure 6. For these experiments, three holes of diameter 0.83 cm (for a total surface area of 1.6 cm^2) and depth 1 cm are drilled into a plastic block and filled with approximately 0.5 g of lithium hydride each. The block is placed in a sealed container, which is held at a constant relative humidity through the use of a saturated salt solutions. Water vapor produced by the saturated salt solution reacts with the lithium hydride; the produced hydrogen is collected in an 1 L inverted graduated cylinder. Five experiments were

run, each at a different relative humidity. The humidities tested are listed in Table 2. Each experiment lasts approximately 10 hours, during which the rate of hydrogen production reaches a rate that is very nearly constant, as reported in literature [29]. The rate of H_2 production is recorded in this constant region.

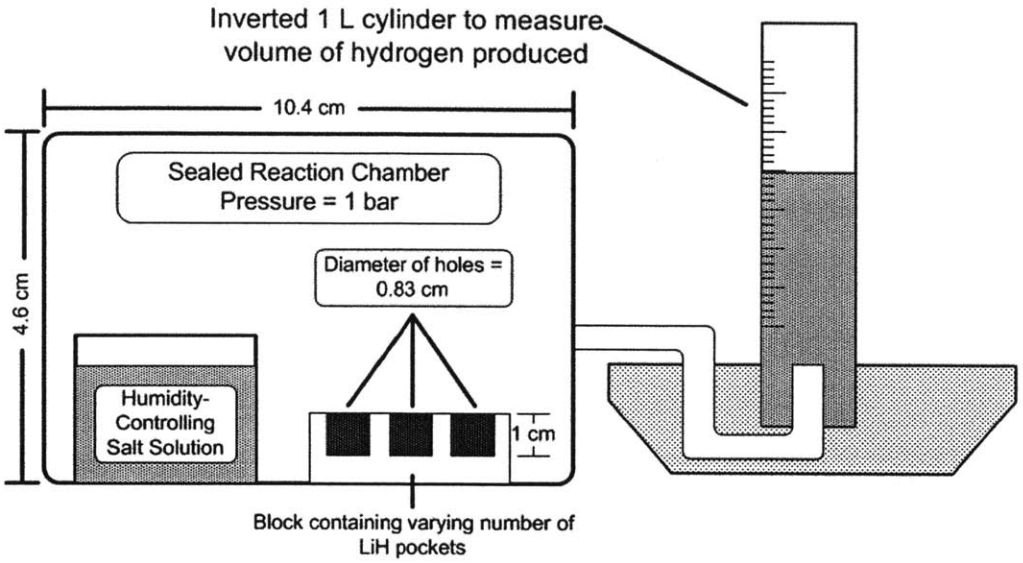

Figure 6: Experimental setup used to demonstrate effect of relative humidity on hydrogen production rate.

Relative Humidity	Salt used to Control Humidity
11%	Lithium Chloride
33%	Magnesium Chloride
53%	Magnesium Nitrate
74%	Sodium Chloride
100%	Water (No Salt Added)

Table 2: Relative humidities to test rate of hydrogen production and salts producing these humidities. These numbers assume the temperature is 20° C [37].

The results of these experiments are compiled in Figure 7. The rate of hydrogen production increases approximately linearly with relative humidity.

A second series of experiments was run that investigated the effect of varying exposed lithium hydride surface area on the rate of hydrogen production. These experiments also used the experimental setup depicted in Figure 6, although with constant humidity set at 34%. Six

holes were drilled in a plastic block (also of 0.83 cm diameter and 1 cm depth). To vary the surface area of lithium hydride, the number of holes filled with hydride was varied from 1 to 6. In each experiment, the relative humidity was held constant by using a solution saturated with magnesium chloride. The results of these experiments are presented in Figure 8. The rate of hydrogen production is roughly linear with increasing surface area.

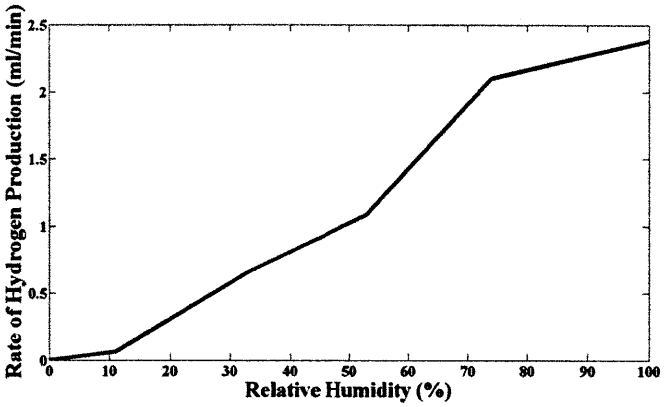

Figure 7: Rate of hydrogen production as a function of relative humidity.

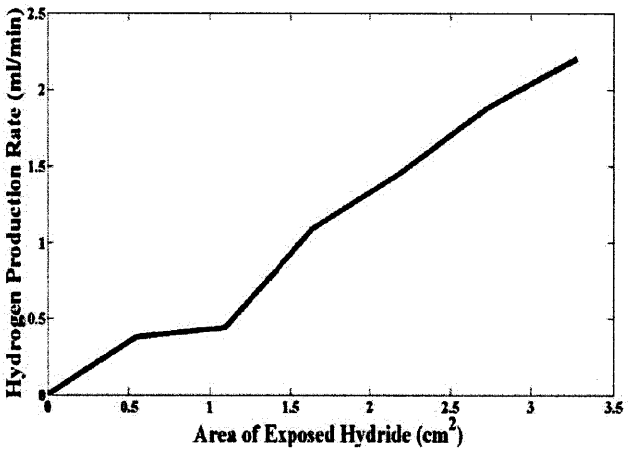

Figure 8: Rate of hydrogen production as a function of surface area.

2.3.3 Total Hydrogen Yield of Lithium Hydride

The third reason lithium hydride was selected for long life, low power fuel cell power systems was its perceived high utilization efficiency. In this thesis, the utilization efficiency is defined as the moles of hydrogen produced over the course of an experiment divided by the

theoretical number of moles contained in a given quantity of lithium hydride. A utilization efficiency of 1 indicates that the hydride has produced its theoretical amount of hydrogen; a utilization efficiency of less than 1 indicates that something has prevented the release of hydrogen. A hydrogen storage source should have a high hydrogen utilization efficiency to avoid wasted system mass and wasted system volume.

According to experiments run in literature, lithium hydride has a high utilization efficiency of above 90% [26]. This research tests the utilization efficiency using an experimental setup similar to that shown in Figure 6. Two experiments were run, labeled A and B in this thesis. In each experiment a flask was filled with a measured quantity of lithium hydride. The initial volumes and masses of the lithium hydride in both of these experiments is presented in Table 3. A source of water vapor at 100% humidity was placed in the sealed container alongside the hydride. Over the next week, the water vapor reacted with the lithium hydride and the volume of hydrogen gas produced was measured. The final volume of hydrogen gas produced is also presented in Table 3. The final volume is the total volume of hydrogen output before the lithium hydride stopped producing hydrogen. Figure 9 shows the reaction's percent completion over time, where 100% corresponds to the theoretical output of hydrogen. The experimental results are close to those presented in [26], which carries out a similar experiment on lithium hydride and determines that lithium hydride has a utilization efficiency of 91%. The results found in [26] are shown in Figure 10.

Experiment	**Initial Mass of LiH**	**Volume of LiH**	**Exposed Surface Area**	**Theoretical H_2 Yield (Liters)**	**Actual H_2 Yield (Liters)**	**Utilization Efficiency (%)**
A	0.8 g	2.79 cm^3	3.98 cm^2	2.42	2.40	99
B	1.4 g	3.78 cm^3	3.98 cm^2	4.23	3.97	94

Table 3: Initial parameters to test whether lithium hydride releases the theoretical amount of hydrogen. The experimental results and percent utilization are contained in the final two columns.

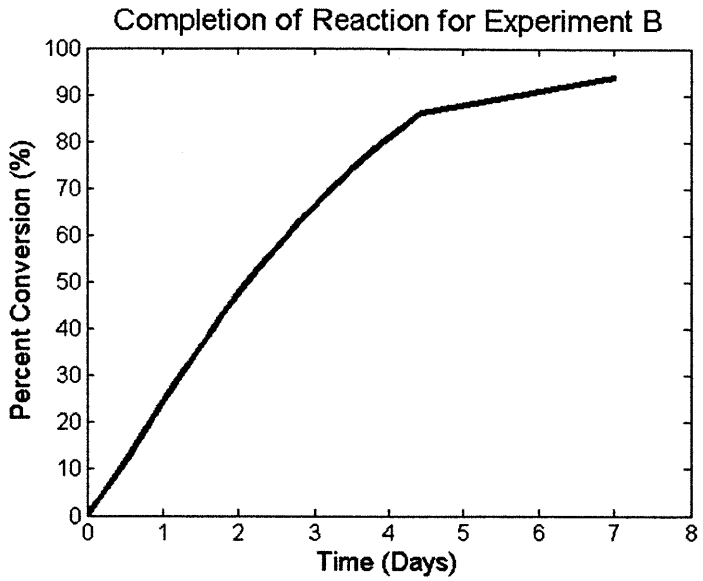

Figure 9: Percent completion of reaction for Experiment B.

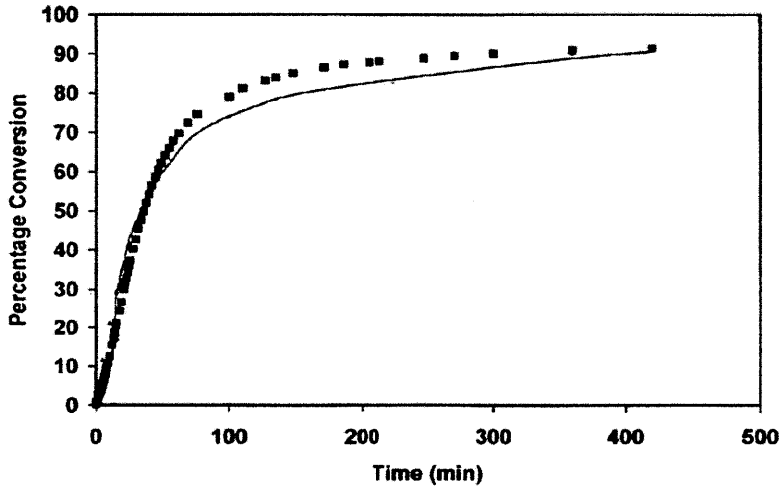

Figure 10: Percent conversion for lithium hydride experiment performed in [26]. Points are experimental data points; the curve is the prediction of a model.

The results of these short term experiments indicate that lithium hydride should be well-suited for high efficiency PEM fuel cell power systems because of its high hydrogen yield. The experiments indicate that over time periods measured in days and for small quantities of lithium hydride (around 1 gram), lithium hydride is able to produce very close to its theoretical content

of hydrogen. This agrees with the tri-layer model which states that a thickening lithium hydroxide layer does not control lithium hydride's ability to produce hydrogen.

The experimental results of this section, 2.3.3, are presented to explain why lithium hydride was chosen for long-life fuel cell systems, although this research (presented in Chapter 5 and 6 of this thesis) shows that the results presented here are incomplete. Experiments discussed in later chapters that are carried out over longer time periods (1-3 months) indicate that the rate of hydrogen production does decrease significantly and that, over significantly long time periods, lithium hydroxide prevents water from reaching the hydride. For this reason, the high hydrogen yield of lithium hydride is the weakest of the three reasons for choosing lithium hydride for use in long life PEM fuel cell power systems.

2.4 Conclusions

Effective hydrogen storage is a difficult problem and a challenge for widespread adoption of hydrogen. Of the many possible solutions, lithium hydride was chosen for this research, which centers on long-life, low-power PEM fuel cell systems. Lithium hydride was chosen because it has a high gravimetric weight efficiency of hydrogen, controlling the reaction is simple, and its actual hydrogen output was very close to its theoretical hydrogen output. As research progressed, it became clear that the third assumption was not entirely correct.

Once lithium hydride was selected as the hydrogen storage medium, it was necessary to design a hydrogen generator, which is discussed in the next chapter.

CHAPTER

3

DESIGN OF A HYDROGEN GENERATOR BASED ON LITHIUM HYDRIDE

The system concept of lithium hydride providing fuel for a hybrid PEM fuel cell system, it was necessary to design a hydrogen generator. This design is carried out with a number of objectives and assumptions.

Assumptions of Hydrogen Generator

1. The system would be operated in terrestrial environments.
2. Environmental temperatures would range from 10-40° C.
3. It was assumed the system would not be used in a very dry environment, i.e. the environmental relative humidity would be greater than 20%.
4. The system would remain stationary and upright.

Objectives of Hydrogen Generator Design

1. Produce hydrogen at a controlled pressure for use in low power PEM fuel cells.
2. Have the ability to produce hydrogen for months or years or at least be scalable to these lifetimes.
3. High hydrogen volume and weight efficiency so that the generator has the potential to be built into a small and lightweight package.
4. Very little to no electrical power consumption because the system is designed for low-power applications.
5. A simple design – a complex design has more components that can fail over a long-lifetime.

The following sections describe the design process that went into each generator iteration as well as experimental results.

3.1 Actively Controlled Designs

The first iteration of hydrogen generators relies on active control. These generators illustrate that it is possible to control the generator's pressure through actuating with liquid water or water vapor.

3.1.1 Peristaltic Pump and Liquid Water Actuation

The first generator design relies on pumping water droplets to activate the hydride; the rate of droplets released into the system is used to control the hydrogen pressure.

One design challenge is to decide how to deliver water into the system. This is because the system requires such low flow rates of water in order to produce the necessary hydrogen. A 250 mW PEM fuel cell system requires 1.46×10^{-6} moles per second of hydrogen (assuming 65% efficiency). Given that the hydrolysis of lithium hydride requires one mole of water for every mole of hydrogen produced, this means that the hydrogen generator would require a water input of 2.62×10^{-5} grams of water per second which equals 2.62×10^{-5} milliliters per second of water, which is a very small amount of water for normal pumps to deliver.

A number of micro-pumps were considered. Microfluidic dispensers were first considered [38]; however, they were not chosen due to cost and difficulty integrating into a mobile system. Commercially available micro-piezo print heads such as those found on a desktop printer [39] were investigated but it was concluded that they would be too complex to control. Micro-piezo pumps were considered but decided against due to the need for an external voltage amplifier [40]. Finally, a small peristaltic pump was chosen. It was selected because of its low-cost, ease of use, and ability to drop small amounts of water (approximately 1 milliliter per second) into the generator.

The peristaltic pump still delivers much higher flow rates of water than required, but it is recognized that it does not need to provide micro-liter flow rates. Instead, the pump releases a droplet of water into the system onto a wick without contacting the hydride. The droplet evaporates and reacts with the hydride over a 30-40 minute time period until another droplet is needed. Using this approach also avoids liquid water touching lithium hydride, which is a violent reaction and can ignite.

The remainder of this initial system is designed as pictured in Figure 11. Lithium hydride is placed into five 10 mL glass beakers, each filled with approximately 0.5 g of hydride. To provide a closed system, the beakers are packed in a sealed chamber (an Otterbox™ was used). The chamber is not perfectly sealed to hydrogen and allows a small amount of gas leakage. This is beneficial to test the controller because it allows the generator's pressure to decrease over time. This mimics the effect of a fuel cell, which would consume the hydrogen.

The control scheme was simple: when the pressure dropped below a pre-determined value, the pump would release a droplet of approximately 50 microliters onto the wick. The droplet would evaporate and react with the hydride.

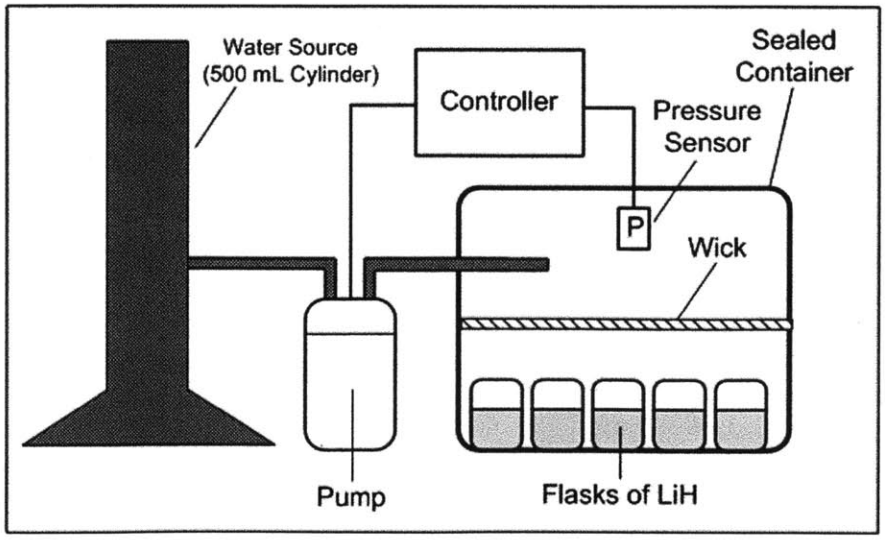

Figure 11: Experimental setup used to actively control hydrogen pressure.

The objective of this experiment was to determine whether the pressure of the lithium hydride could be controlled at a pre-determined operating point within an error bounds. For the purpose of this experiment, the operating point was set to 110 kPa with error bounds of ±1 kPa. The results of the experiment are presented in Figure 12 and Figure 13.

Figure 12 presents the graph of pressure over time. Each vertical line represents a point at which the pump delivered a droplet into the system. From the plot, it is evident that the system was able to control the pressure at the set point of 110 kPa and within the error bounds. The pressure signal exhibited periodic oscillations, with one droplet of water released every 40 minutes.

Figure 13 plots the system pressure and humidity on the same graph. The pressure and humidity rise at regular intervals; a droplet is introduced into the system, the droplet evaporates, and the water vapor subsequently reacts with the lithium hydride. The peaks of the humidity always occur before the peaks in pressure. This trend is reported in literature and relates to the difference between the time when the water vapor is absorbed by the hydride bed and when it reacts with the lithium hydride [18].

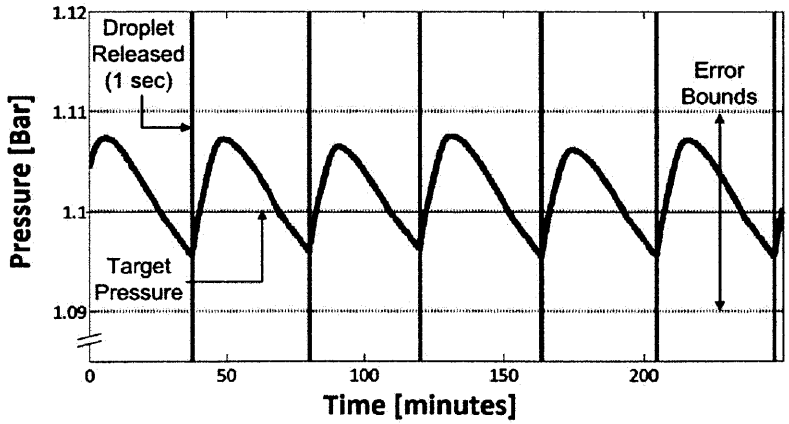

Figure 12: Graph of pressure versus time which demonstrates control of system pressure at 1.1 bar.

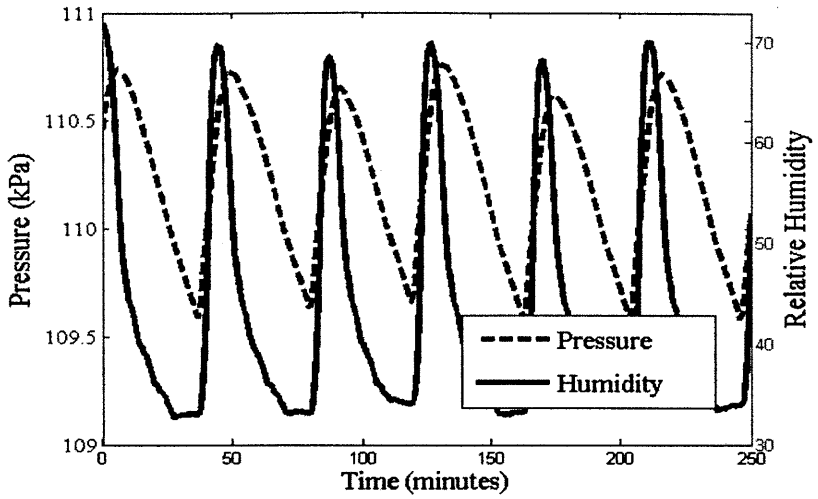

Figure 13: Plot of system humidity and pressure during controlled experiment.

3.1.2 Water Vapor Actuation

The next set of generator experiments focus on actuating using only water vapor. This is done to make the system more efficient and versatile. To activate the hydride, the peristaltic pump design requires a source of liquid water. This means that liquid water must either be carried with the power system or obtained from the environment. Storing liquid water in the fuel cell system increases system weight and reduces weight efficiency. Obtaining water from the environment (assuming water is not readily available in the sensor's surroundings) means condensing water vapor, which is energetically expensive. Using only water vapor to activate the hydride avoids these difficulties. Water vapor is available in significant amounts almost anywhere on earth.

3.1.2.A Servo Actuator in Combination with Nafion Membrane Part 1

The second design still implements three key new design elements: actuation relying only on water vapor, the use of a valve mechanism, and includes Nafion as a water transport medium.

Relying only on water vapor to activate the hydride raised the question of how to input water vapor into the system. Initially, pumping water vapor with the same peristaltic pump from the previous design was attempted but too was energetically expensive to be feasible. Instead, it was concluded that a valve mechanism would be most efficient. When the generator pressure

dropped below a certain value, the valve would open to allow water vapor to enter the generator from the environment, otherwise, the generator would be closed.

To build a valve, it was necessary to have a membrane that allowed for water vapor to enter the system but prevented hydrogen from escaping. This behavior is exhibited by a material already present in PEM fuel cells: Nafion. Nafion is a polymer that was developed by DuPont in the 1960s and comes as a clear, thin plastic-like sheet. It is rugged and has a chemical structure similar to Teflon [41]. In PEM fuel cells, Nafion serves as the proton transport membrane which transports protons from the anode to the cathode. A mathematical description of Nafion's transport properties are given in Chapter 4, but what is important for the development of a hydrogen generator is the fact that it allows water to pass much more easily than it does hydrogen or other system gases such as nitrogen. Therefore Nafion can be used as a gateway, which allows water to enter but maintains the generator's internal hydrogen pressure. This is depicted in Figure 14.

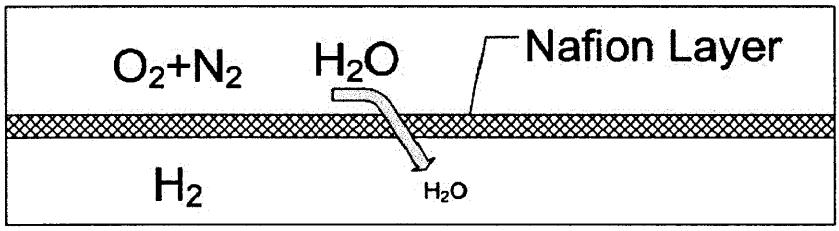

Figure 14: Mass transport in Nafion membrane.

Nafion will transport water from regions of higher water partial pressure to regions of lower water partial pressure. This means that Nafion can transport water from regions of lower total pressure to regions of higher total pressure, as long as there is a decrease in water partial pressure. This feature is depicted for two sealed chambers in Figure 15. This characteristic is good for the design of a hydrogen generator because it means that Nafion can deliver water

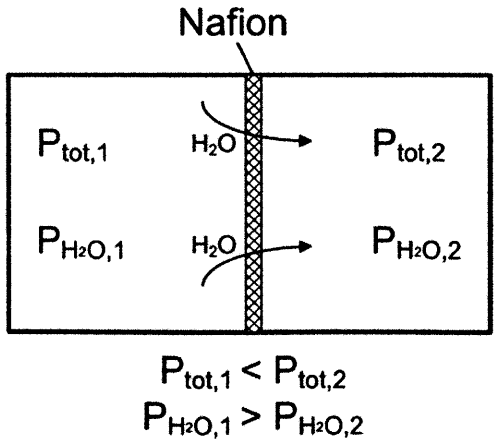

Figure 15: Ability of Nafion to transport water to regions of higher total pressure

vapor from the environment into areas of higher hydrogen pressure. The type of Nafion use for the designs presented in this thesis is Nafion 117.

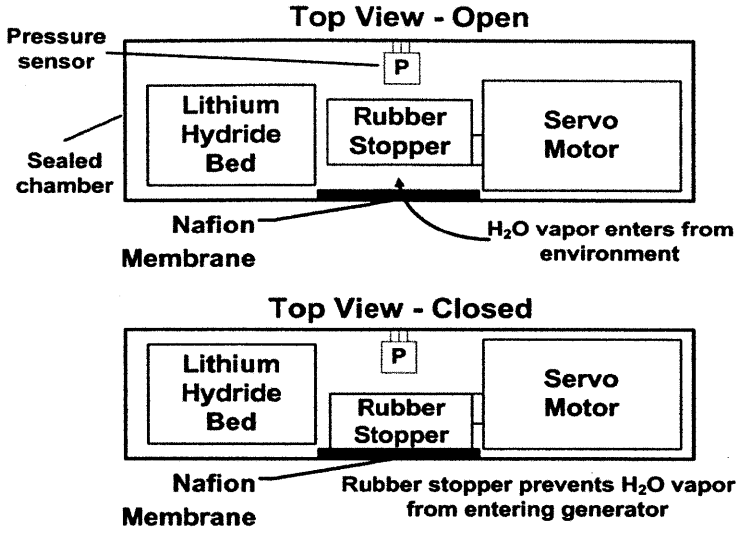

Figure 16: Diagram of mechanism that would control pressure by opening and closing a valve.

The first design that utilized Nafion to transport water vapor into the system is pictured in Figure 16. A rubber stopper was attached to a servomotor that acted as a valve to water vapor. If the pressure inside the generator was too high, the servo would press the rubber stopped against the Nafion, which was intended to prevent water vapor from entering the system. If the pressure were too low, the servo would open the valve and allow water vapor to enter the system and react with the bed of lithium hydride.

The valve's ability to control humidity within the generator was tested. The results of this test are presented in Figure 17. The plot shows the relative humidity inside the generator with the valve open versus the humidity with it closed. The results indicate that Nafion allowed water to enter the system. Unfortunately, whether the plug was open or closed, the humidity within the device rose considerably. This indicated that the valve was unable to prevent water vapor from entering the device and, therefore, would be unable to control the hydride reaction. A better seal was necessary and this was the focus of the next design.

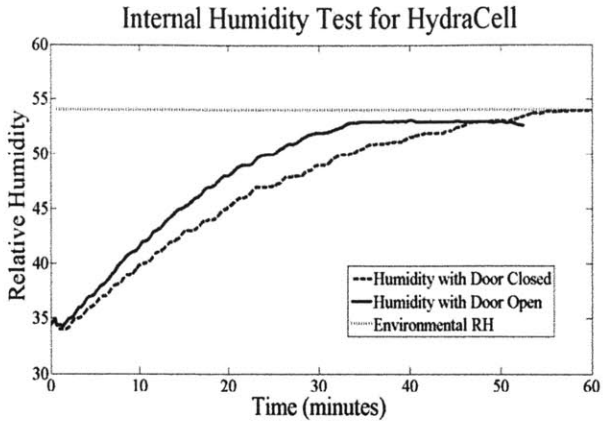

Figure 17: Graph of humidity versus time for valve open and valve closed.

3.1.2.B Servo Actuator in Combination with Nafion Membrane Part 2

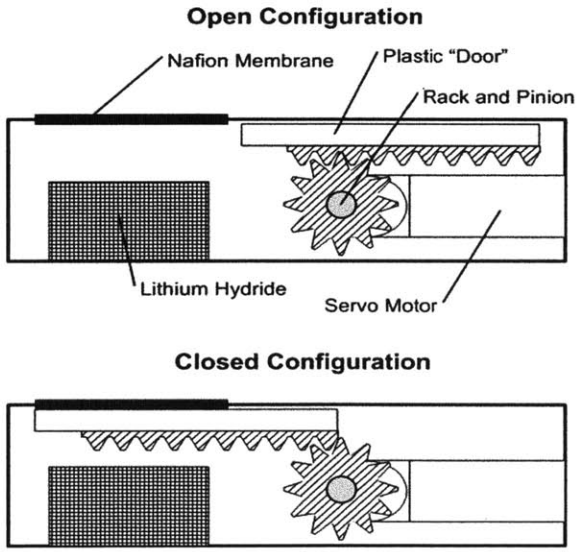

Figure 18: Third iteration of active hydrogen generator.

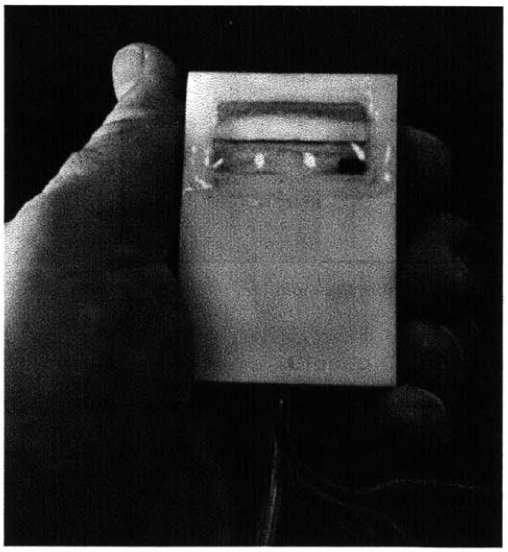

Figure 19: External view of third iteration.

The next iteration of the vapor-actuated hydride system had the goal of producing a valve that could effectively block humidity from entering the system when closed. This was accomplished through use of a precisely-machined Plexiglas door, which would open upon commands to a servomotor. The servo's rotational motion was translated into linear motion

through the use of a rack and pinion gear. The system design is presented in Figure 18. An image of the generator is in Figure 19. The image shows the generator's Nafion membrane, glued to the outside of the generator. In the image, the Plexiglas door is halfway open.

This iteration was tested for its ability to control relative humidity and pressure. The results of these tests are shown in Figure 20 and Figure 21. Due to the precisely machined assembly holding the Plexiglas door in place, this system exhibited much better performance than previous iterations. As shown in Figure 20, there was a significant difference between the rate of rise of system humidity with the door closed as with it open. After establishing humidity control, the generator was filled with approximately 2 grams of hydride and tested for its ability to control pressure. Figure 21 presents a plot of the controlled system pressure versus time. The operating point was arbitrarily set at 105 kPa, which the generator is able to maintain after rising from atmospheric pressure. This experiment was run using only atmospheric humidity (approximately 30%) to generate hydrogen. The blip on the pressure graph near the 10 minute mark represents a droplet of water that was dropped on the Nafion surface. If the droplet of water were a disturbance, the generator was able to successfully reject it; the pressure did not become unstable and returned to 105 kPa within 10 minutes. Finally, this system design accomplished the goal of reducing the pressure oscillations seen with the first design discussed. After the initial rise and disturbance, the pressure oscillates much less than the system using a peristaltic pump.

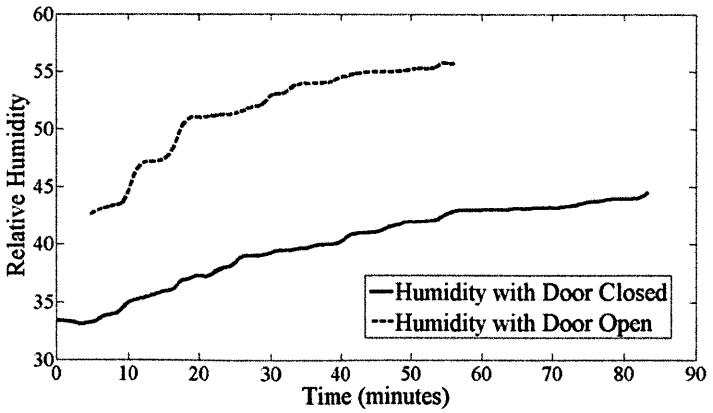

Figure 20: Comparing humidity rise inside third iteration with door closed and with door open.

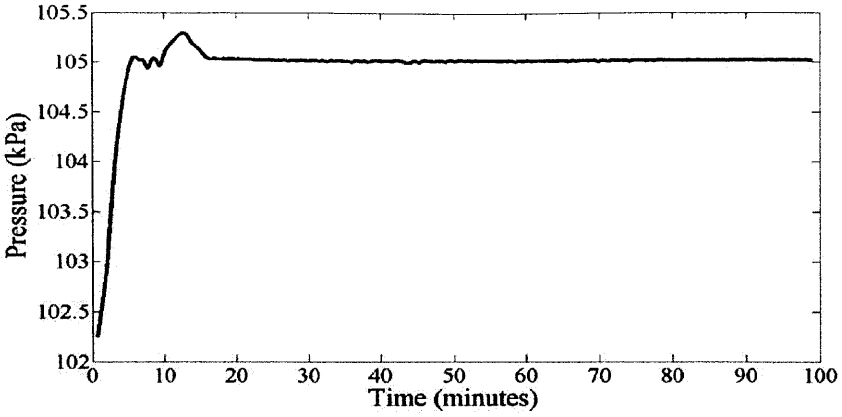

Figure 21: Pressure response of third iteration. Pressure controlled at 105 kPa.

3.2 Passively Controlled Designs

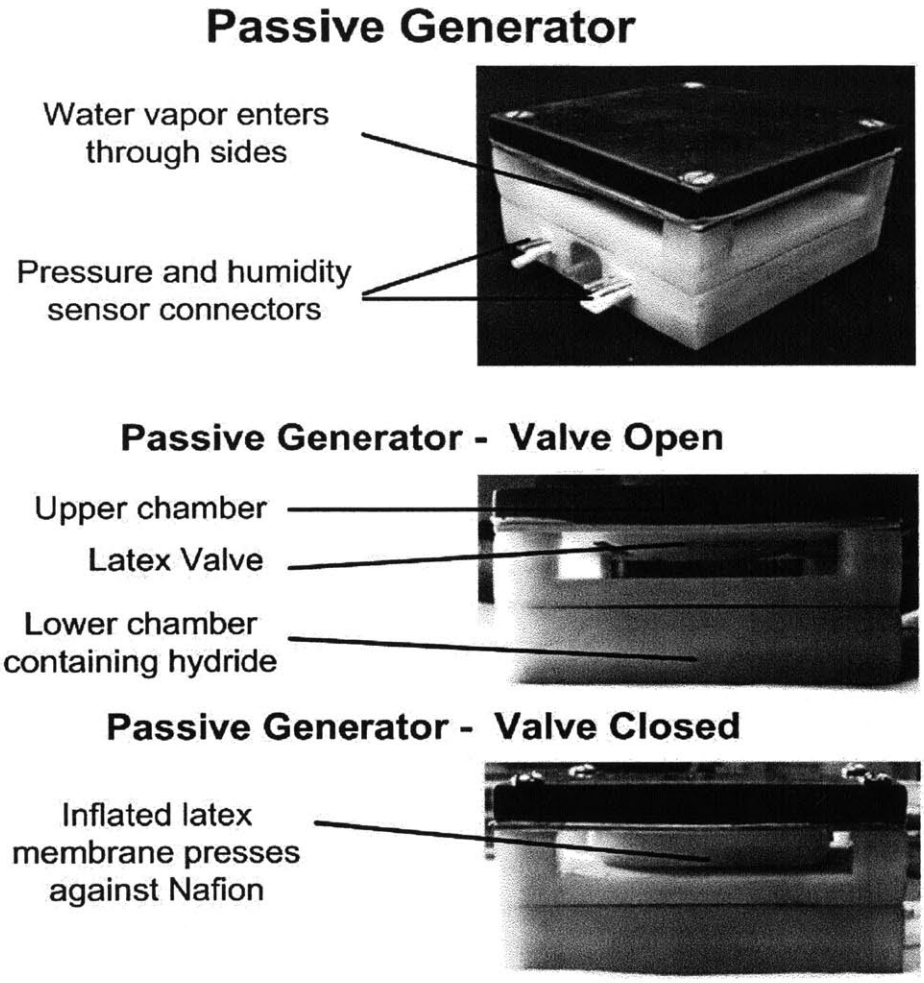

Figure 22: Photographs of the passive hydrogen generator with valve open and closed.

A passive generator offers the benefit of simplicity and low parasitic power consumption. Both of these features are important for long-life, low power missions: simplicity means less components are prone to failure and no parasitic power consumption translates into higher efficiency. For this study, a passive hydrogen generator was conceived utilizing the following features:

a. Water transport using a Nafion membrane, similar to its use in the active designs
b. A compliant mechanism that acts as a valve

To passively control the hydrolysis reaction, a compliant latex membrane is used. This membrane uses pressure feedback and works similarly to a valve. When the system pressure is above the operating point, the membrane presses against the Nafion layer and prevents water vapor from entering the system. When the pressure is low, the latex membrane pulls back and allows water to enter the system and activate the hydride.

The passive hydrogen generator consists of two chambers. A lower chamber contains a bed of lithium hydride. Water is allowed to enter the lower chamber through a Nafion membrane, which is placed above the hydride. A second chamber, which is connected to the first to allow pressure communication, contains a latex membrane. Hydrogen pressure generated by the hydride inflates the latex, which then presses against the Nafion membrane and prevents water vapor from entering the system. A detailed description of the device is shown in Figure 22 and Figure 25. Figure 22 contains three photographs of the passive generator. The top photograph shows the overall generator and how water enters the device. The bottom two photographs show the latex valve mechanism when it is open (allowing water vapor to enter the system) and closed (blocking water vapor from entering the system). A complete description of the generator's control mechanism is presented in the series of cross-sectional views in Figure 25, on page 37.

Latex was chosen as the complaint valve mechanism because of its resilience (it permanently deforms very little over prolonged use). An advantage of latex is that it is easy to alter the mechanism's compliance by selecting a thicker or thinner membrane (a latex sheet of thickness 0.012" was used in these experiments). Latex has the disadvantage of allowing a small percentage of the produced hydrogen to diffuse into the environment. Tests done on the generator described in this thesis indicate that the leak rate was less than 5% of the hydrogen produced while running at 250 mW.

The short term passive hydrogen generator was experimentally studied by itself and in a fuel cell system. The pressure response of the isolated hydrogen generator (not connected to the fuel cell) is shown in Figure 23. Note that the pressure overshoots before returning to a constant pressure of approximately 130 kPa (the operating points chosen for this experiment are arbitrary). The time response is second order and exhibits oscillations before coming to the equilibrium pressure. The dynamic behavior will be explored in greater detail in the mathematical model developed in Chapter 4. Figure 24 presents the pressure response of the

passive hydrogen generator powering a 50 mW fuel cell system over the course of approximately 24 hours. The generator is able to hold the hydrogen pressure at 119 kPa within error bounds of approximately ±1 bar.

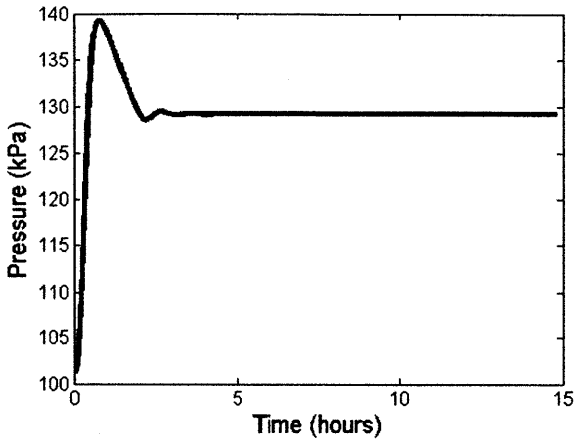

Figure 23: Pressure response of passive generator isolated from fuel cell.

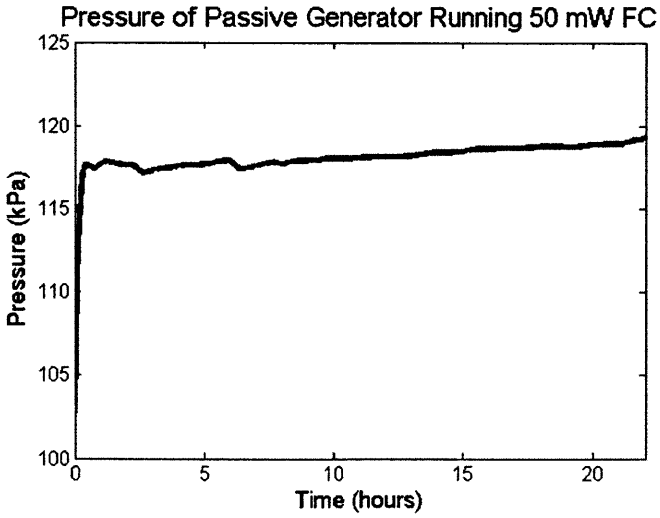

Figure 24: Pressure plot of the passive generator running 50 mW fuel cell system.

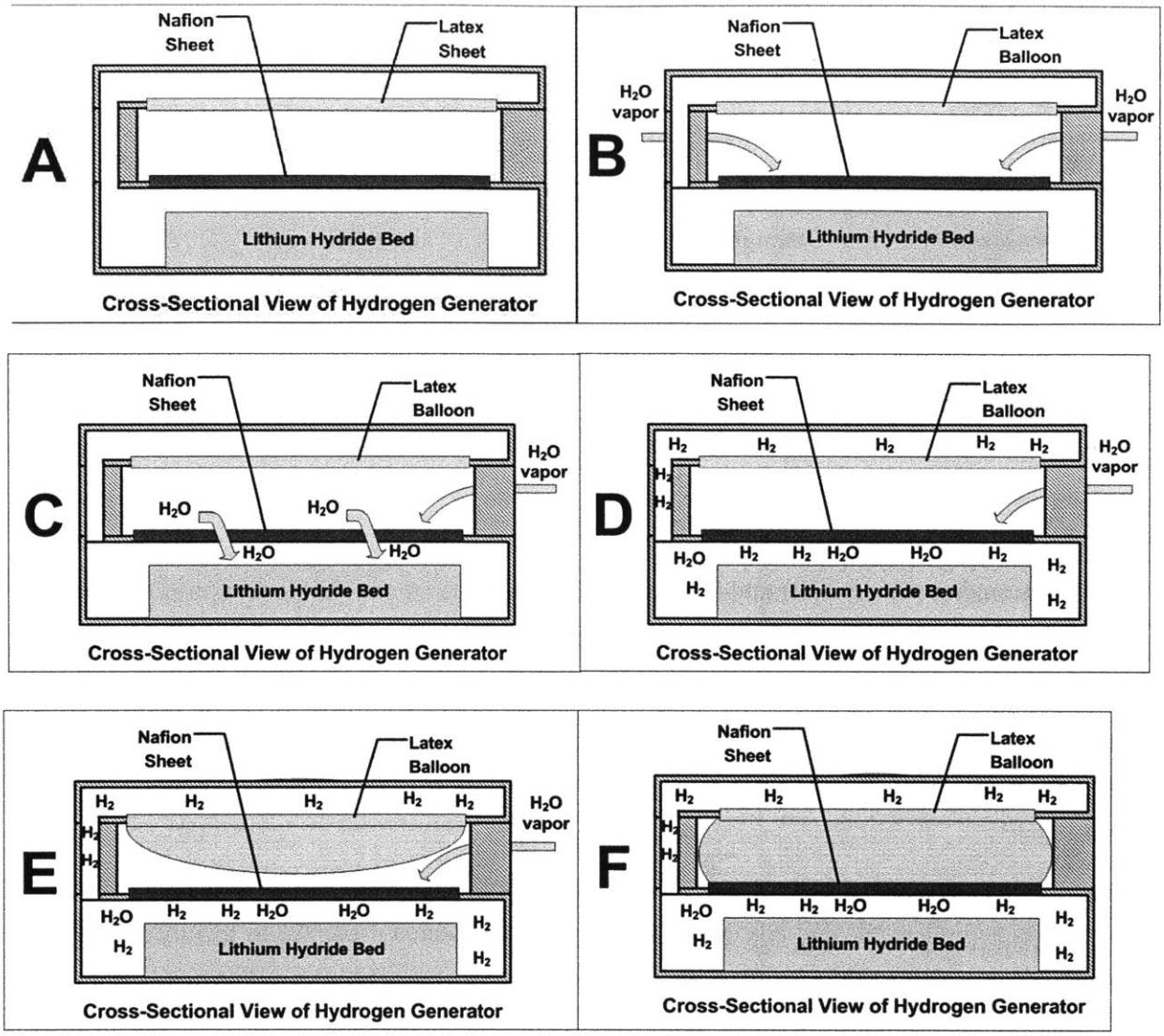

Figure 25: Description of passive control mechanism for hydrogen generator. **A)** The hydrogen generator is divided into two chambers, a lower chamber that holds the hydride bed and an upper chamber bounder by a latex sheet. A channel allows pressure communication between the chambers. **B)** Water vapor enters through the sides of the device from the atmosphere to fill the space between the chambers. **C)** Water vapor diffuses across the Nafion sheet and into the bottom chamber. The Nafion allows water vapor to enter but allows very little hydrogen to escape. **D)** Water vapor reacts with the lithium hydride and fills the bottom and top chambers. **E)** Hydrogen pressure in the top chamber inflates the latex sheet. **F)** The latex sheet inflates and presses against the Nafion sheet underneath. It serves as pressure feedback because it prevents more water vapor from entering the device.

3.3 Conclusions

This chapter describes the design process for the hydrogen generator based on lithium hydride. The work presented demonstrates that it is possible to design active and passive control modules that regulate the hydrogen pressure at an operating point. The remainder of this thesis focuses on the passive design because of its simplicity and efficiency. After development of the generator, the focus shifted to modeling the generator's dynamics and experimentally validating the generator and lithium hydride in a long life (3 month) experimental system. These topics are the subjects of the next two chapters.

3.3.1 A Note on Operating Pressure

Throughout this chapter and thesis the operating generator operating pressures are chosen arbitrarily. Selecting an optimal operating pressure is a non-trivial task. Higher hydrogen pressures increase performance by improving the fuel cell's reaction kinetics, which are described by the electrochemical Butler-Volmer equation. Lower hydrogen pressure means less hydrogen loss from factors including hydrogen diffusion across the fuel cell's polymer membrane.

Determining the ideal pressure is an optimization problem that depends on fuel cell geometries and other relevant physical parameters. The research presented in this thesis did not consider this optimization. Therefore, operating pressures were chosen arbitrarily as "reasonable" values; these are values high enough to avoid hydrogen starvation and low enough to avoid significant hydrogen leaks (105 kPa – 120 kPa).

CHAPTER

4

DYNAMIC MODEL OF THE PASSIVE HYDROGEN GENERATOR

A dynamic model of the passive hydrogen generator proposed in Chapter 3 is developed. The purpose of this model is to explain the generator's short-term pressure response. Future research on the passive generator can use the model as a tool to optimize the generator's design.

4.1 Overview and Assumptions of Model

The objective of the model is to accurately predict the passive generator's short-term pressure in response to external relative humidity and fuel cell power demand. The work presented in this chapter models the system response over short time periods (less than 1 day). This model does not consider the effect of lithium hydroxide on the rate of hydrogen production

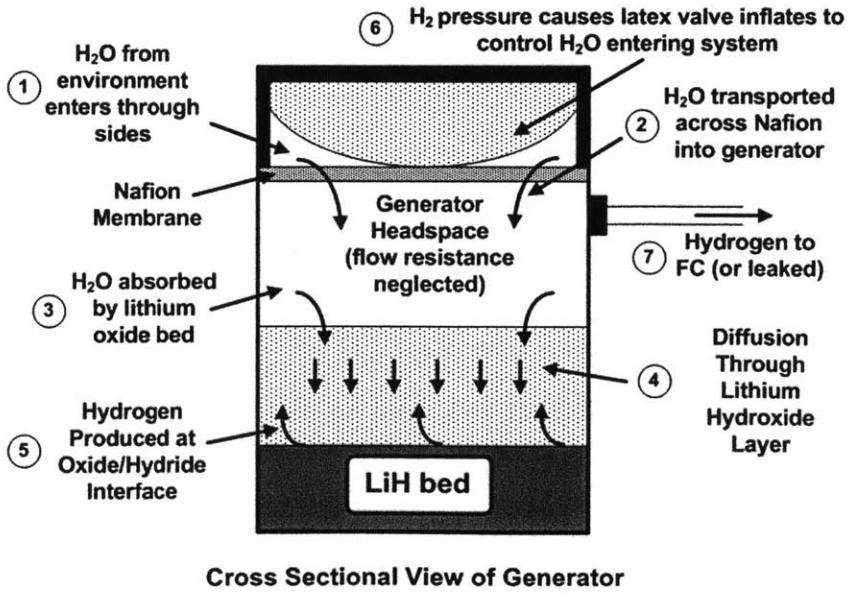

Figure 26: Components taken into account to model passive hydrogen generator. Numbers correspond to numbers in text.

over longer periods (1-3 months). Lithium hydroxide buildup is important to the design of a long term generator and is investigated in Chapter 6.

To simplify the model while capturing the system's essential dynamics, the generator's dynamics are broken down into a number of subcomponents. These components are shown in the cross-section view presented in Figure 26. They include:

1. Water vapor from the environment diffuses along the gap between the Nafion membrane and latex sheet.
2. Water vapor enters the generator through the Nafion sheet.
3. The top layers of lithium hydroxide absorb water vapor in the generator's headspace.
4. The water vapor diffuses through the hydroxide layer toward the hydride.
5. Water vapor reacts with lithium hydride to produced hydrogen gas.
6. Hydrogen production increases the generator's pressure, which inflates the latex valve. The valve presses against the Nafion membrane and reduces the surface area for water to enter the system.
7. Hydrogen leaves to a fuel cell or through small leaks in the device.

Additional assumptions are made in the model, they include:

1. Diffusion of across the Nafion sheet (Labeled 1 in Figure 26) is two dimensional, and diffusion of water inside the generator is one dimensional.
2. The relative humidity is constant within the hydrogen generator's headspace.
3. The system remains upright and temperature constant.
4. The thickness of the lithium hydroxide layer and its diffusivity remain constant. This is reasonable for simulations of less than 1 day but breaks down for longer time periods. This phenomenon is the subject of Chapter 6.
5. All water molecules sufficiently "close" the lithium hydride react with the hydride. In terms of this model, close means the discretization cell next to the lithium hydride. This is in accordance with the experimental observation that the relative humidity next to a bed of pure lithium hydride is approximately zero.
6. The lithium hydroxide does not store water and lithium hydroxide monohydrate does not form.

4.2 Components of Model

4.2.1 Diffusion of Water into System

The model's first component is diffusion of water vapor across the top of the generator from the environment. This process in shown in Figure 27. Because there is a significant absorption of water into the Nafion along the flow channel, it is reasonable to question whether diffusion or convection drives mass transport. To determine this, the non-dimensional Peclet Number is used, where:

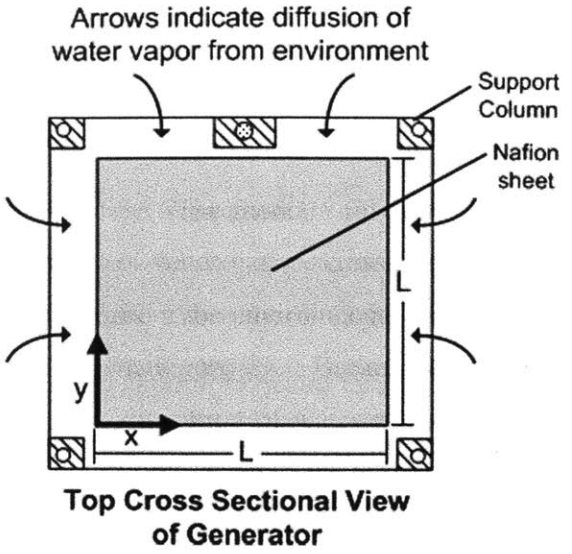

Figure 27: Top cross sectional view of generator showing how water enters the system.

$$Pe_L = \frac{LU}{D} \tag{6}$$

The Peclet number measures the relative importance of convection to diffusion. In this equation, L represents a characteristic length in the system which is taken as one of the generator's sides, U represents a characteristic velocity, which is computed to be the velocity of water vapor required to supply a 250 mW fuel cell system operating at 60% efficiency, and D is the diffusivity of water vapor in air, which depends on temperature. For this system, the Pecelet number is computed to be:

$$Pe_L = 0.003 << 1 \tag{7}$$

Because this is much less than 1, it is assumed that diffusion dominates the flow across the top of the generator and is modeled by the two dimensional diffusion equation with a sink term:

$$\frac{\partial C}{\partial t} = D\frac{\partial^2 C}{\partial x^2} + D\frac{\partial^2 C}{\partial y^2} - \dot{C}_{abs}(x, y, t) \tag{8}$$

where C is the concentration of water vapor as a function of x, y, and t. The coordinates x and y are shown in Figure 27. The first two terms on the right-hand side of this equation represent diffusion terms and the third term represents the water vapor which enters the generator through

the Nafion membrane. The boundary conditions for this partial differential equation assume that the humidity at each of the boundaries is the environmental relative humidity. This is written mathematically as:

$$C(x, y=0, t) = C(x, y=L, t) = C(x, y=0, t) = C(x, y=L, t) = \frac{\phi_{amb} P_{sat}}{RT} \tag{9}$$

4.2.2 H_2O Transport Through Nafion

To model the water transport through the Nafion membrane, a model developed in [42] is used. The moles of water passing through the Nafion per unit surface area is:

$$N_w = -\frac{\rho_M}{M_M \sigma_M} \int_{\lambda_1}^{\lambda_2} D_w d\lambda \tag{10}$$

where ρ_M is the Nafion's density, M_M is the molecular weight of the Nafion, σ_M is the thickness of the Nafion. D_w is the Ficikian diffusion coefficient, presented as

$$D_w = 3.10x10^{-3} \lambda(-1+e^{0.28\lambda}) \exp\left[\frac{-2436}{T}\right] \tag{11}$$

The temperature is given as T and λ is the Nafion's water content, which ranges from 0 (for perfectly dry membranes) to 22 (for wet membranes). It is provided by

$$\lambda = 0.043 + 17.81a_w - 39.85a_w^2 + 36.0a_w^3 \tag{12}$$

where a_w is the activity of water. The activity of water relates to the relative humidity on each side of the Nafion:

$$a_w = \frac{\Phi_{avg}}{100} \tag{13}$$

where Φ_{avg} is the average relative humidity on each side of the Nafion. Equations (10), (11), and (12) show transport of water through the Nafion is higher when the Nafion has a higher water content, i.e. Nafion transports water better when it is wet.

4.2.3 Diffusion of H_2O Through Lithium Hydroxide/Lithium Oxide Layer

The amount of water absorbed by the lithium hydride/hydroxide bed was determined experimentally as a function of relative humidity inside the generator and the surface area of lithium hydride. This expression is given as:

$$\dot{n}_{H_2O,absorbed} = (1.79*\phi - 8.42)*A_{LiH}*(4.5\text{e-}8) \tag{14}$$

where the left-hand side represents the molar flow rate of water into the hydroxide bed, Φ is the relative humidity of the generator's headspace, and A_{LiH} is the exposed hydride surface area (which remains constant). This relationship assumes that the lithium hydroxide does not absorb water and that lithium hydroxide monohydrate does not form.

Water transport across the hydroxide layer is modeled as one dimensional diffusion, which requires Fick's law of diffusion:

$$\frac{\partial C}{\partial t} = D\frac{\partial^2 C}{\partial x^2} \tag{15}$$

where C measures concentration of water vapor and D is the diffusivity. For Eq. (15), two boundary conditions are required and one initial condition. At the top of the lithium oxide layer ($x=0$), the flux of water is known from Eq. 14. Mathematically,

$$J\Big|_{x=0} = -D\frac{\partial C}{\partial x}\Big|_{x=0} = -\frac{\dot{n}_{H_2O,absorbed}}{A_{LiH}} \tag{16}$$

Where J represents the flux at $x=0$. The right-hand side must be divided by the area of the lithium hydride bed to translate a molar mass flow rate to flux. For the second boundary condition, the concentration at the Li_2O/LiH interface was assumed to be a zero, as the water at this point would react with the lithium hydride:

$$C\Big|_{x=depth} = 0 \tag{17}$$

Finally, the initial condition is zero concentration of water throughout the lithium oxide layer:

$$C(x, t=0) = 0 \tag{18}$$

The diffusion equation was discretized using a Crank-Nicolson scheme, where the second order derivative on the right-hand side can be approximated by the trapezoidal rule [43]

$$\frac{T_i^{n+1}-T_i^n}{\Delta t}=\frac{D}{2}\left[\frac{T_{i-1}^n-2T_i^n+T_{i+1}^n}{h^2}+\frac{T_{i-1}^{n+1}-2T_i^{n+1}+T_{i+1}^{n+1}}{h^2}\right] \tag{19}$$

if we set

$$r=\frac{D\Delta t}{2h^2} \tag{20}$$

we can relate the nodes at time n with time $n+1$ through the system of equations:

$$\begin{bmatrix} 1+2r & -r & 0 & 0 \\ -r & 1+2r & -r & 0 \\ 0 & \ddots & \ddots & \ddots \\ 0 & 0 & -r & 1+2r \end{bmatrix}\begin{bmatrix} T_2 \\ T_3 \\ \vdots \\ T_{N-1} \end{bmatrix}^{n+1}=\begin{bmatrix} 1-2r & r & 0 & 0 \\ r & 1-2r & r & 0 \\ 0 & \ddots & \ddots & \ddots \\ 0 & 0 & r & 1-2r \end{bmatrix}\begin{bmatrix} T_2 \\ T_3 \\ \vdots \\ T_{N-1} \end{bmatrix}^{n} \tag{21}$$

This expression allows us to march through time and update each node in the simulation.

4.2.4 Mass Balances

There are two important states within the generator: the number of moles of water vapor and the number of moles of hydrogen. For each species, one can write mass balance of the form:

$$\dot{n}_i=\sum_k \dot{n}_{i,in}-\sum_k \dot{n}_{i,out}+\dot{n}_{i,gen} \tag{22}$$

where the left-hand side represents the change in number of mole of species i, and the right-hand side represents the mass inflows and outflows with a generation term due to the system's chemical reaction. For water vapor, this term is negative, while for hydrogen the generation term is positive. For the water vapor within the generator, this balance takes the form:

$$\dot{n}_{H_2O}=\dot{n}_{H_2O,Nafion}-\dot{n}_{H_2O,absorbed} \tag{23}$$

where the left hand side is the change in the number of moles of water within the generator, and the right hand side represents the water entering through the Nafion membrane minus the water

vapor absorbed by the hydride bed. The amount of water consumed by the hydride reaction as a function of surface area and relative humidity is contained in Eq. (14).

A rate equation for the molar balance of hydrogen can be written:

$$\dot{n}_{H_2} = \dot{n}_{H_2,gen} - \dot{n}_{H_2,F.C.} - \dot{n}_{H_2,leak} \tag{24}$$

where the three terms on the right hand side correspond to the generated hydrogen, the hydrogen consumed by the fuel cell, and the inherent leakage rate for the generator, which was measured to be about 5% of the total hydrogen produced for a 250 mW fuel cell.

4.2.5 Modeling the Effect of Pressure on Latex Sheet

The latex sheet controls the pressure by inflating and restricting the Nafion surface area available to transport water into the system. A model is necessary that relates the generator's internal pressure to the surface area available for water transport. The effect of pressure on the latex membrane was modeled in two ways. First, an empirical model was created that relied on inflating the generator to various pressures, recording the amount of surface area coverage, and fitting a polynomial to the data. This worked well to model the generator that was built, but does not work well when designing new devices with different geometries. Therefore, a second model is presented that relies on principles of hyperelasticity. The second model can be used to design future devices.

4.2.5.A Method A: Empirical Model

Experiments were run to determine the relationship between generator pressure and the area of latex pressed against the Nafion sheet. Subtracting this closed-off area from the total Nafion area, gives the area open for water transport.

As shown in Figure 28, the hydrogen generator was inflated to a specific pressure and the x and y projections of the latex sheet

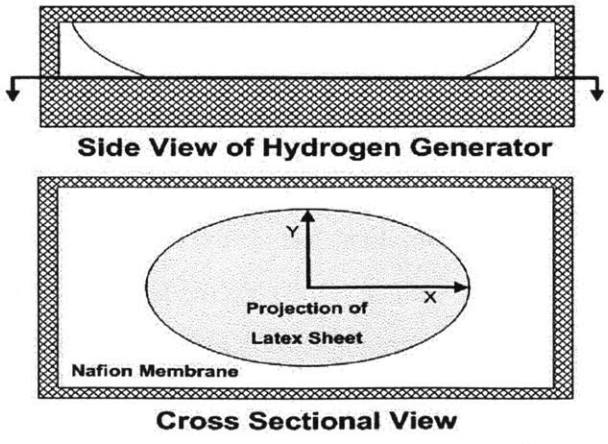

Figure 28: Diagram of measurements that led to relation between pressure and coverage area of Nafion membrane for method A.

pressed against the Nafion were recorded. The x and y measurements were then related to the pressure through a second-order polynomial as given in Equations (25) and (26):

$$x = -0.031 * P^2 + 7.19 * P - 409.24 \tag{25}$$

$$y = -0.0043 * P^2 - 0.76 * P + 32.20 \tag{26}$$

It was assumed that the projection of the latex membrane onto the Nafion membrane formed an ellipse. The total projected area of the latex membrane pressed against the Nafion is related by the equation for the area of an ellipse given the lengths of its major and minor axes:

$$A_{closed} = \pi * x * y \tag{27}$$

This area corresponds to the surface area closed off to water diffusion. Therefore, the area allowed for water diffusion into the system is given by

$$A_{open} = A_{total} - A_{closed} \tag{28}$$

4.2.5.B Model of Latex Membrane Based on Hyperelasticity

The second relationship between the generator's pressure and the valve's area was determined from physical principles. This model is included in the thesis because it will help inform future generator designs, especially ones with different geometries.

Modeling rubber deformation can be very complex. The model presented here uses simple principles of hyperelasticity presented in [44]. To model pressure's effect on the latex membrane, a relationship between the stress and strain is necessary. In particular, the generator's compliant valve involves biaxial stretching of the latex, or stretching along the membrane's surface. One such model is the model of a Mooney-Rivlin material, in which elastic coefficients do not depend on principle stresses. For a Mooney-Rivlin material, the relationship between stress and strain is given as:

$$\tau_{\lambda\lambda} = \left(\lambda^2 - \frac{1}{\lambda^2 \mu^2}\right)\left(s_+ - s_- \mu^2\right) \tag{29}$$

$$\tau_{\mu\mu} = \left(\mu^2 - \frac{1}{\lambda^2\mu^2}\right)\left(s_+ - s\_\lambda^2\right) \tag{30}$$

In these equations λ and μ are the strains tangent to the membrane surface such that the normal vectors parallel to λ and μ are orthogonal to the normal of the membrane's surface. Both to λ and μ are normal to one another. Similarly, $\tau_{\lambda\lambda}$ and $\tau_{\mu\mu}$ are the corresponding strains parallel to these stresses. Finally, s_+ and s_- are elastic coefficients and properties of the material.

A simple relationship between the membrane's stress and the generator's pressure is achieved through a force balance between the pressure force and the stress over the membrane's cross-section. This relationship is:

$$\tau = \frac{P \cdot r}{2 \cdot t} \tag{31}$$

where P is the generator's gauge pressure in Pascals, r is the unstretched surface area of the balloon, and t is the thickness of the latex. Given the strains defined by Eq. (29) and (30), it is necessary to determine the balloon's geometry. As shown in [44], the most stable form for a balloon to take is a sphere – real balloons deviate from a spherical shape due to varying latex thickness. It is assumed that the latex membrane used in the hydrogen generator follows this behavior. The strains in Equations (29) and (30) (λ and μ) have the effect of increasing the radius of the sphere from its unstretched radius. Using this simple model, solving for the new latex geometry (and the valve closure area) is a three step process:

1. For a given generator pressure, determine the stress using Equation (31).
2. Solve for the strains using Equations (29) and (30).
3. Determine the balloon geometry using the strains, assuming that the unconstrained balloon will always form a spherical shape.

The hyperelastic model was simulated in Matlab for a wide variety of generator pressures and the amount of Nafion surface area coverage was recorded. To compare the results against the empirical model, the simulations used the same geometry used to generate the empirical model. The results are presented in Figure 29. Both models produce similar values for similar pressures, although the shapes of the curves are considerably different. In future generators, the design should consider the hyperelastic model since the empirical model was fit to one generator.

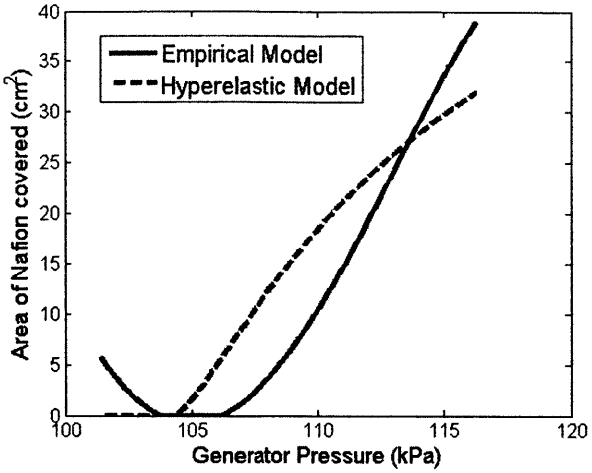

Figure 29: Comparison of valve coverage for both models.

4.3 Simulations

To validate the model, a simulation was run for an isolated generator (not connected to a fuel cell) at 50% environmental relative humidity. The results are presented in Figure 30 compared against the pressure response of the actual system.

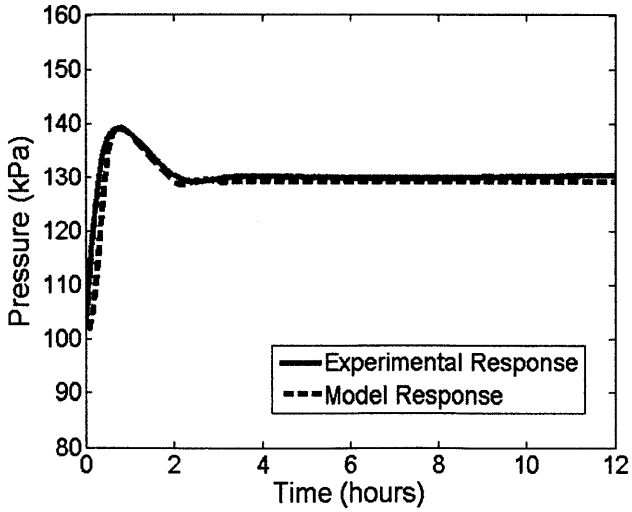

Figure 30: Pressure response of model versus experimental pressure response.

4.3.1 Case Study: Effect of Actuator Saturation on Control

The model can be used to predict the generator's ability to reject disturbances and demonstrate how actuator saturation diminishes the generator's ability to control pressure. Two simulations were run, each used the same generator geometry and parameters. In Simulation One, the generator is supplying a fuel cell operating at 25 mW. In Simulation Two, the generator is powering a fuel cell running at 250 mW. Both simulations experience a step change in environmental relative humidity from 55% to 35%. A summary of the simulations and experiments are presented in Table 4. The pressure responses versus time for each simulation are shown in Figure 31 and Figure 32. The change in relative humidity has a much greater effect on Simulation Two, the generator producing 250 mW of hydrogen. The reason is due to actuator saturation. The generator in Simulation Two must compensate for the drop in ambient relative by opening up a larger surface area of Nafion than the generator in Simulation One; this causes the pressure to drop more.

Simulation	FC Power Demand	Change in Humidity	Initial Operating Pressure	Final Operating Pressure	Pressure Change
One	25 mW	20%	117.9 kPa	116.7 kPa	1.2 kPa
Two	250 mW	20%	113 kPa	105.5 kPa	7.5 kPa

Table 4: Table summarizing results of two simulations.

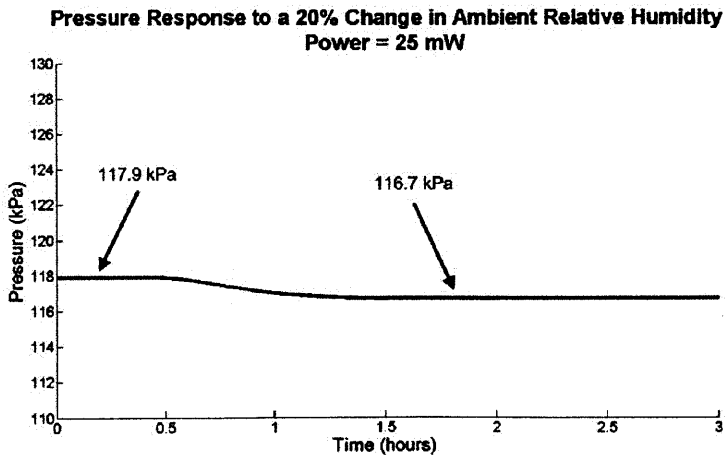

Figure 31: Pressure response for Simulation One.

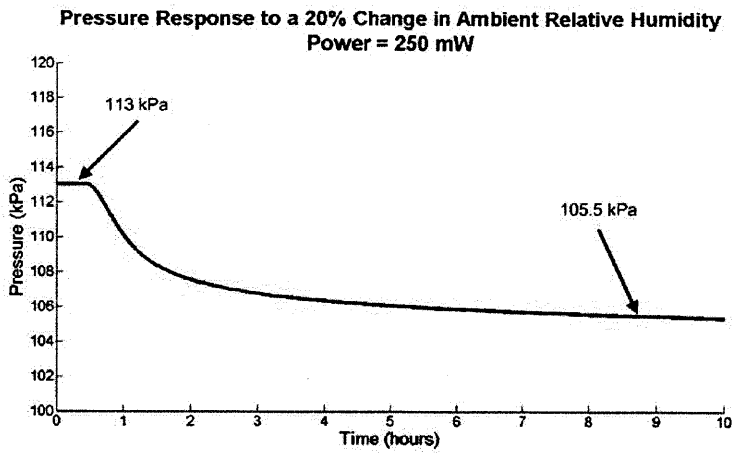

Figure 32: Pressure response for Simulation Two

4.4 Conclusions

In this chapter, a model for the short-term dynamics of the passive hydrogen generator is presented. The model was developed to explain the generator's pressure response. The model can be used to build an optimized passive hydrogen generator and predict the generator's ability to control pressure. To properly design a long term generator, this model must be combined with the long experimental results for long term lithium hydride hydrolysis presented in Chapter 6.

4.4.1 A Note on Constants

To enable the continuation of this work in the future, all constants and parameters used in the above simulations are included as part of Appendix C.

CHAPTER

5

BENCH TOP FUEL CELL SYSTEM

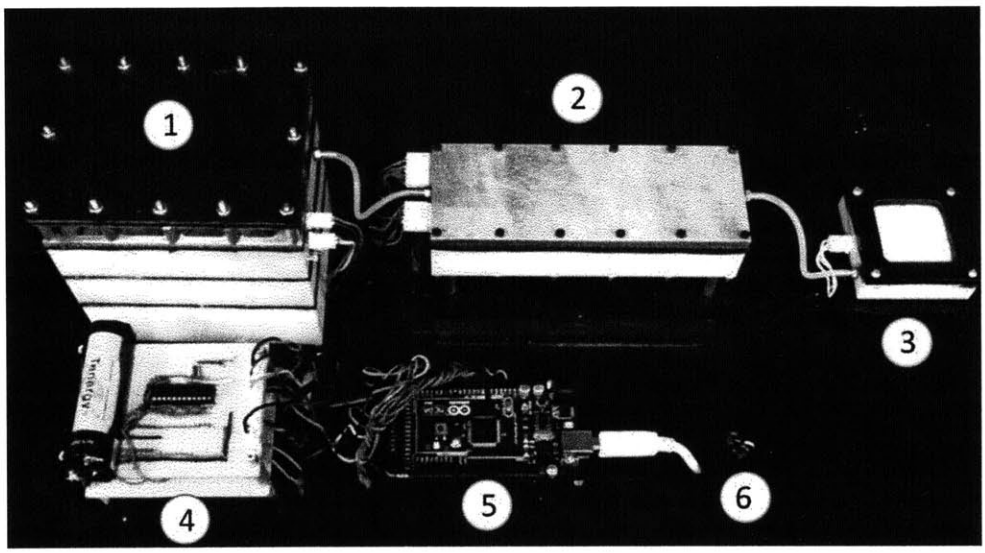

Figure 33: Benchtop fuel cell system. **1.)** Hydrogen generator **2.)** Fuel cell block enclosing 5 fuel cells. **3.)** Nitrogen removal subsystem **4.)** Power Electronics. **5.)** Data collection equipment **6.)** Demonstration load

Lithium hydride has been widely discussed for its potential as a source of hydrogen for PEM fuel cells. It has not been experimentally studied in a long-life, low-power fuel cell system. Therefore, a benchtop experimental system, pictured in Figure 33, was built. The research objective of this benchtop system was to experimentally study the passive hydrogen generator described in Chapter 3 as well as test the suitability of lithium hydride for long-life, low-power systems. The goal was to run the experimental system for three months at an average power of 250 milliwatts. To simulate the varying power demand of a sensor network, the load would operate on a 10% duty cycle. The system would run until either three months or the fuel cells no longer produced power. The components of the system are described next.

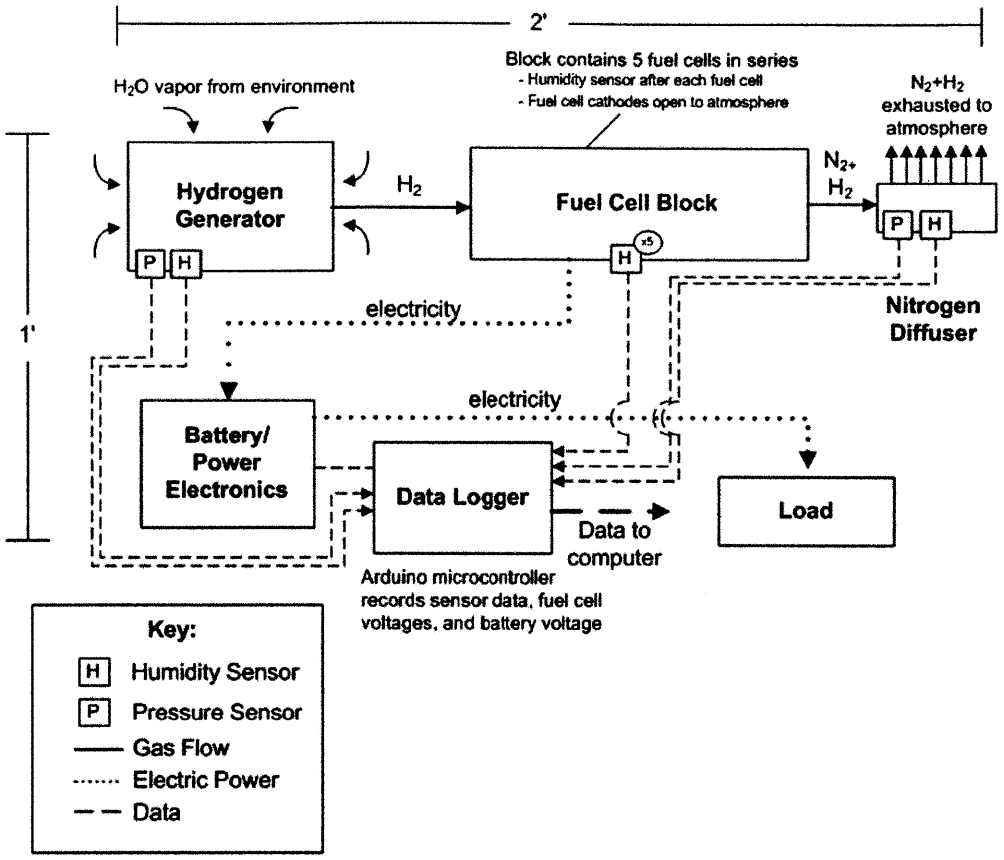

Figure 34: Diagram detailing gas flows, power flows, and sensor data in benchtop fuel cell system.

5.1 System Components

The relevant gas flows, electric power flow, and sensor data connections of the benchtop experimental system are shown in Figure 34. The dimensions of each component are included in Appendix D. Each of the components will be described in the following sections.

5.1.1 Lithium Hydride Hydrogen Generator

The hydrogen generator used the passive latex valve mechanism as presented in Chapter 3. No attempt was made to optimize the geometry of this device for the benchtop system.

5.1.2 Fuel Cell Stack

The fuel cell stack consisted of five fuel cells obtained from Horizon Fuel Cell Technologies, Ltd, product number FCSU-012. The fuel cells were connected in series so that the voltage of each individual fuel cell as well as the system's voltage could be recorded. Humidity sensors were built into the aluminum manifold to obtain the humidity of each fuel cell's anode. Each fuel cell's cathode received air from the surrounding environment.

5.1.3 Nitrogen Removal Subsystem

The nitrogen removal subsystem released passively released nitrogen that built up in the anode chamber during dead-ended anode operation. This phenomenon will be discussed in detail in Chapter 7. The nitrogen removal subsystem consisted of layers of polystyrene foam that would allow anode gases (both nitrogen and hydrogen) to diffuse from the anode into the atmosphere. This would prevent nitrogen from building up in the anode chamber and choking the fuel cells.

5.1.4 Power Electronics

To mimic a sensor network, the system's load operated on a 10% duty cycle. Because varying load voltage is harmful to the fuel cell, a battery must be placed between the fuel cell and the load. The battery chosen for this system was an A123 Nano-Phosphate battery. The fuel cell charged the battery and the oscillations only affected the battery.

5.1.5 Arduino Microcontroller

To record sensor data, an Arduino Mega 2560 microcontroller was used to relay system data to the computer.

5.1.6 Load

To simulate the behavior of a sensor network, a simple DC motor was used as a load. A switching transistor ensured that the load would be on a 10% duty cycle.

5.2 Experimental Results

After approximately twenty-five days, the fuel power began to decrease. Due to experimental error in measuring the power, it cannot be stated with certainty that the fuel cell was originally running at 250 mW. The microcontroller is believed to have consumed power and therefore it can only be said that the original power was between 250 and 410 mW. However, it can be said with certainty that the power decreased after the first three weeks. The battery's decreasing voltage was evidence of this; the battery was slowly losing charge without being replenished. To prevent degradation of the fuel cells, an electronic switch was implemented where the microcontroller would disconnect the load from the fuel cells whenever the battery voltage became too low. During these periods, power from the fuel cells only charged the battery and did not run the motor.

A plot of periods during which the motor was disconnected is shown in Figure 35. Gray areas in this plot represent days on which the motor was disconnected from the battery. White areas indicate periods where the system was charging the battery and running the motor. It is clear from Figure 35 that the system ran the motor less and less as the experiment progressed. This indicates that fuel cell's power output was decreasing. After approximately 57 days, the system could no longer power the motor and the fuel cells only produced enough power to charge the battery.

Ambient humidity was artificially increased through the use of humidifiers in hope that increased humidity would increase the rate of hydrogen production from the lithium hydride. This did not solve the problem of decreasing fuel cell power.

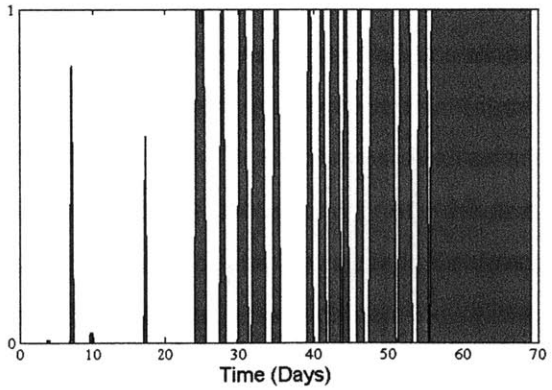

Figure 35: Motor switching on and off during experiment. Gray areas represent times when motor was *not* connected to the fuel cell.

Plots of results for the experimental system are presented in Figure 36, Figure 37, Figure 38, and Figure 39. Figure 36 shows the pressure of the hydrogen generator. Because of the negligible flow resistance that separated the fuel cells and the hydrogen generator, this would also be the pressure seen by the fuel cells. After an initial period of elevated pressure, the generator's pressure oscillated around 102 kPa for the majority of the experiment. The oscillations are due to saturation of the passive actuator; once the hydrogen generator was unable to maintain sufficient pressure to operate the passive actuator effectively, the pressure was uncontrolled and subject to environmental disturbances such as changes in relative humidity. Finally, the pressure shows an abrupt drop-off around the 60 day mark resulting in total loss of power. The pressure drop suggests that the fuel cells underwent hydrogen starvation.

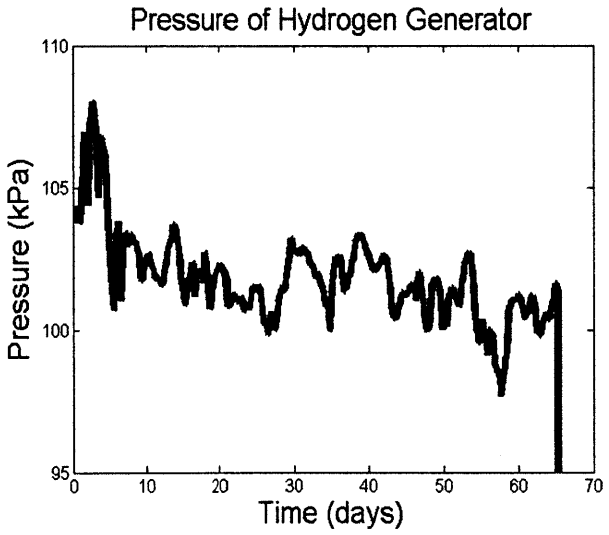

Figure 36: Plot of hydrogen generator pressure versus time.

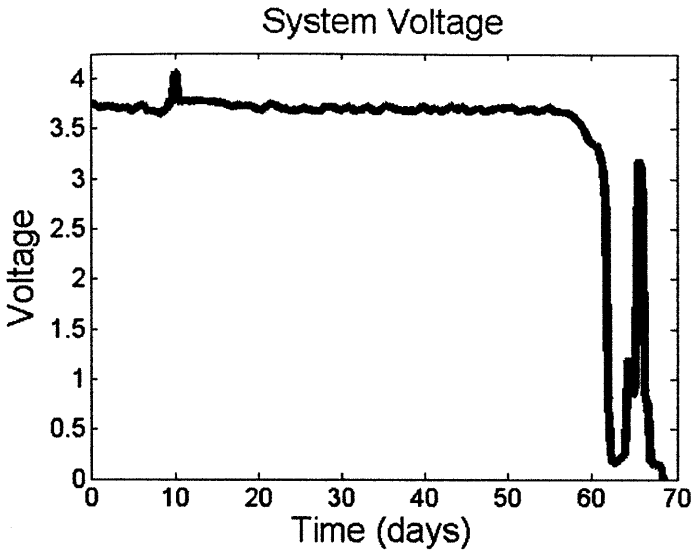

Figure 37: Plot of system voltage as a function of time

Figure 37 presents the voltage of the fuel cell system over the course of the experiment. The system was able to maintain a fairly constant voltage for the first 60 days of the experiment. At approximately 60 days, decreasing hydrogen pressure caused the voltage to crash.

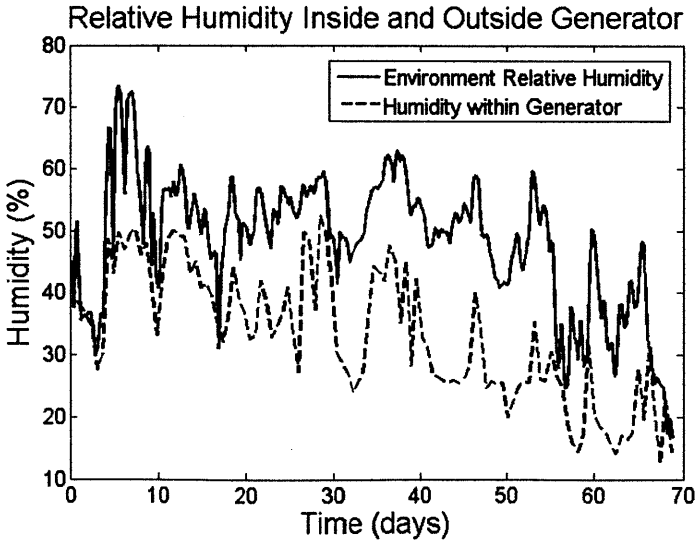

Figure 38: Relative humidity inside the hydrogen generator plotted alongside ambient relative humidity.

In Figure 38, the relative humidity inside the hydrogen generator alongside the ambient relative humidity is plotted. As one would expect, the relative humidity inside the generator always trailed the ambient relative humidity. The difference between the generator relative humidity and ambient relative humidity did not significantly change over the course of the experiment, which indicates the Nafion did not lose its ability to transport water.

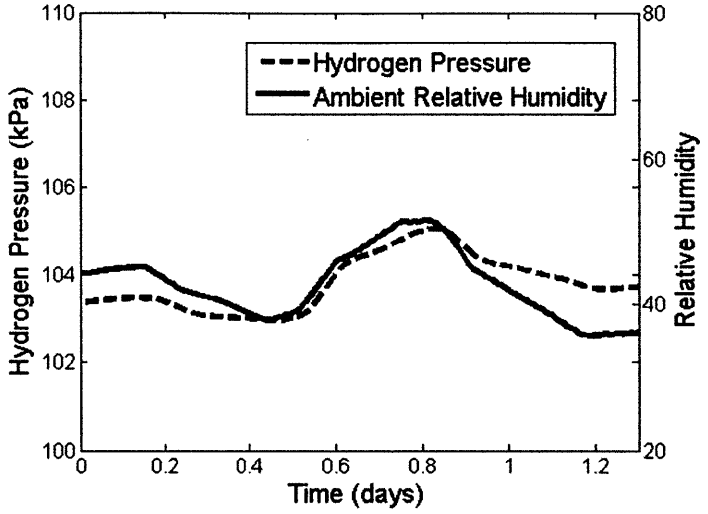

Figure 39: Humidity's effect on pressure during first day of experiment.

There is only a clear relationship between system pressure and ambient humidity during the first few days of the experiment, as shown in Figure 39. In this figure, the pressure follows the ambient humidity closely. However, this trend does not exist for the majority of the experiment. This indicates that changing ambient relative humidity (at least within values ranging from 30-60%) did not have a significant effect on hydrogen production.

5.3 Post-Experiment Analyses

Each component of the experiment was analyzed to determine the cause of hydrogen starvation. The hydrogen generator's Nafion membrane was tested to determine whether its ability to transport water had been reduced during the course of the experiment. The experimental setup to test the Nafion is pictured in Figure 40. In this experiment, Chamber 1 was held at a constant humidity of 76% using a saturated salt solution. Chamber 2 was flushed with dry hydrogen until it reached a low humidity (approximately 20%). A sheet of Nafion was placed between the two chambers. The humidity rise in Chamber 2 was measured. The results of this experiment are given in Figure 41 . In less than ten minutes, the humidity in the "dry" chamber rose to within 10% of the control humidity. This indicated that the Nafion had not lost its ability to transport water.

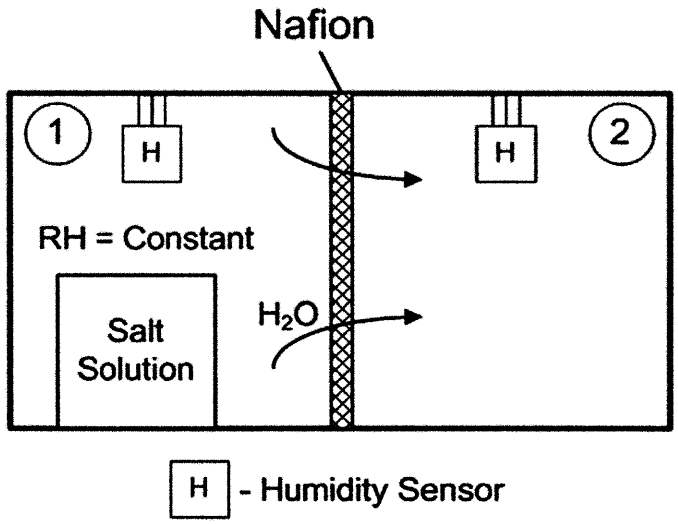

Figure 40: Experimental setup to test Nafion's ability to transport water.

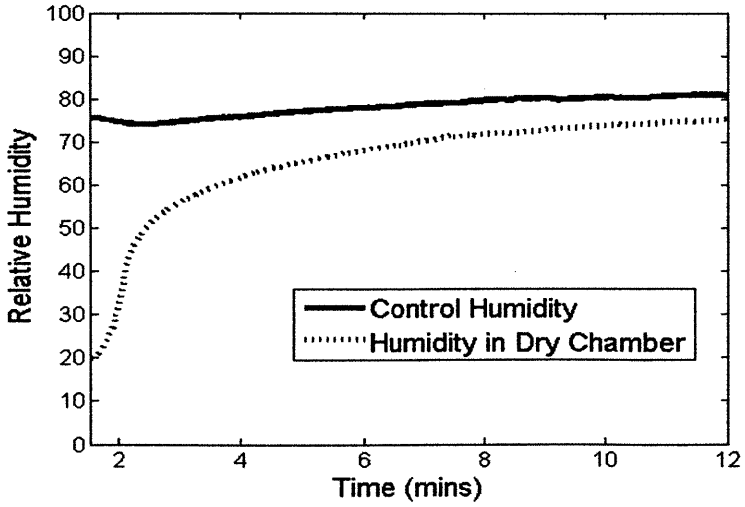

Figure 41: Test of Nafion membrane's ability to transport water post-experiment.

The hydrogen generator was disassembled to determine whether it had caused failure. A picture of the disassembled generator is shown in Figure 42. The generator could cause hydrogen starvation in two ways: the generator could run out of lithium hydride to produce hydrogen or something had prevented the full utilization of the lithium hydride in the generator. The hydrogen generator's post-experimental contents were analyzed. The results of this analysis are presented in Table 5. When dismantling the hydrogen generator, care was taken to analyze each layer of hydroxide and to note any differences in consistency and density. The results of this analysis are presented in Table 6.

Figure 42: Hydrogen generator post-experiment with hydride bed exposed.

	Pre-Experiment Mass (grams)	**Post-Experiment Mass (grams)**
Generator Weight (no hydride)	494.4	494.4
Total Weight	657.2	751.0
Lithium Hydride Weight	162.8	114.0
Byproduct Weight (LiOH)	N/A	140.6

Table 5: Masses of components of the hydrogen generator subsystem, pre- and post-experiment.

Depth (cm) below Nafion Membrane	Density (g/cm^3)	Qualitative Comments
1.72	0.105	White, clumps, many holes
2.84	0.267	White, resembles flour or talcum powder
4.50	0.258	Very similar to above layer
5.46	0.493	Darker, traces of LiH, noticeably harder than above layers
5.81	0.546	Darker, harder, need to apply greater force to break apart

Table 6: Table describing layers of hydroxide found when dismantling hydrogen generator.

Of the original 162.8 grams of lithium hydride placed into the generator, 114.0 grams remained. (This number should be considered a slight underestimate because, although care was taken to separate them, unreacted lithium hydride was mixed with the bottom layers of lithium hydroxide). This means that 48.8 grams of lithium hydride reacted for 30% utilization of the original hydride. The hydrolyzed lithium hydride created 140.6 grams of lithium hydroxide. This is short of the 147 grams of hydroxide that 48.8 grams of lithium hydride should theoretically produce. The difference is most likely due to measurement error due to hydride/hydroxide mixing mentioned above. One can conclude that the majority of the byproduct was anhydrous lithium hydroxide and not lithium hydroxide monohydrate, since 48.8 grams of lithium hydroxide would produce approximately 257 grams of the monohydrate, which is much greater than what was observed.

The byproduct lithium hydroxide powder increased in density with depth as shown in Table 6. In this table, depth is measured as the distance below the Nafion membrane. The powder became more dense with depth because of the weight pressing down from above layers. Qualitatively, the topmost hydroxide was completely white and powdery, while the hydroxide closest to the remaining hydride was harder and darker since it was mixed with hydride.

CHAPTER

6

LONG-TERM HYDROLYSIS OF LITHIUM HYDRIDE

The results of the benchtop system presented in Chapter 5 indicate that lithium hydride's ability to produce hydrogen decreases considerably as the reaction progresses. This is contrary to the original assumption discussed in Chapter 3, where it was assumed that the lithium hydride would be able to produce hydrogen at a constant rate over the course of the experiment and that the reaction would reach close to 100% completion. The buildup of lithium hydroxide on top the lithium hydride is the most probable cause for this decrease.

Understanding the effect of lithium hydroxide on the rate of hydrogen production is extremely important for the design of a long-life hydrogen generator. Therefore, the final part of this research was spent evaluating the long-term evolution of the hydrogen production rate through a series of experiments. The objective of these experiments was to quantify the hydride's decreasing production rate and determine if and how it is linked to the formation of lithium hydroxide.

6.1 Description of Experiments

Tables 7 and 8 provide overviews of the experiments. The experimental setups are detailed in Figure 43, Figure 44, Figure 45, and Figure 46. Experiments 1-3 (labeled A, B, and C in this report) use similar experimental setups. A 100 mL graduated cylinder is filled with compressed lithium hydride to the 55 milliliter mark. A chamber containing a source of water vapor is sealed to the top of the cylinder. The water evaporates and diffuses into the cylinder until reacting with the hydride. The produced hydrogen is output into another graduated cylinder and its volume is continuously measured. The advantage of this design is that it allows for observation of the lithium hydride/hydroxide interface.

Humidity sensors are held at different heights above the hydride. These sensors allow measurement of the humidity gradient that forms between the water source and hydride surface.

The experiments test lithium hydride under different conditions. Experiment A exposes the hydride to water without salt, which means that the humidity in the sealed chamber reaches 100%. Experiment B exposes the hydride to a saturated salt solution of magnesium nitrate that maintains the humidity at 53%. Experiment C holds the system pressure at 1.1 bar to determine the effect of pressure on the hydrogen production rate.

Upon conversion to lithium hydroxide, lithium hydride can expand up to 4-5 times its original volume. The fourth experiment, labeled Experiment D, tests the potential to compress the byproduct lithium hydroxide and reduce system volume. Instead of allowing the hydroxide to freely expand as in experiments A-C, a sheet of Nafion 117 is placed above the lithium hydride. The Nafion allows water vapor to enter the chamber and react with the hydride, but presses against the lithium hydroxide and constrains its ability to expand. To prevent hydroxide from bursting the Nafion, the Nafion membrane is mounted 1.9 centimeters above the hydride to begin the experiment.

Experiment Title	Source Humidity	Pressure	LiOH Constrained
A	100%	1 bar	No
B	53%	1 bar	No
C	100%	1.1 bar	No
D	100%	1 bar	Yes

Table 7: Summary of the four long-term experiments.

Experiment	Mass of Hydride (g)	Volume of Hydride (cm^3)	Density of Hydride (g/cm^3)	Surface Area of Exposed LiH (cm^2)
A	24.5	55	0.45	5.27
B	24.5	55.5	0.44	5.27
C	24.6	55	0.45	5.27
D	5.8	9.52	0.61	4.97

Table 8: Initial masses and densities of lithium hydride in the four experiments.

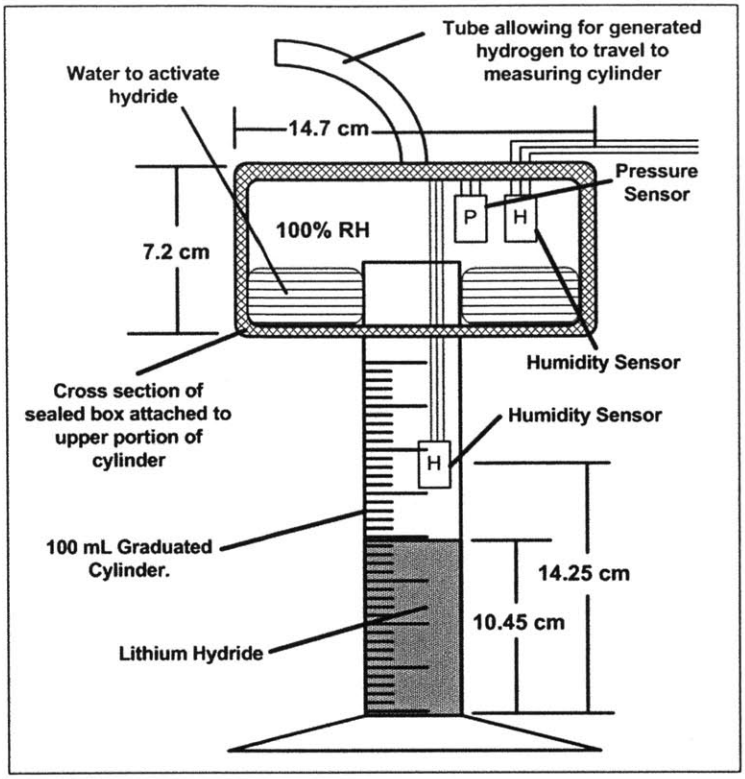

Figure 43: Initial experimental configuration of Experiment A.

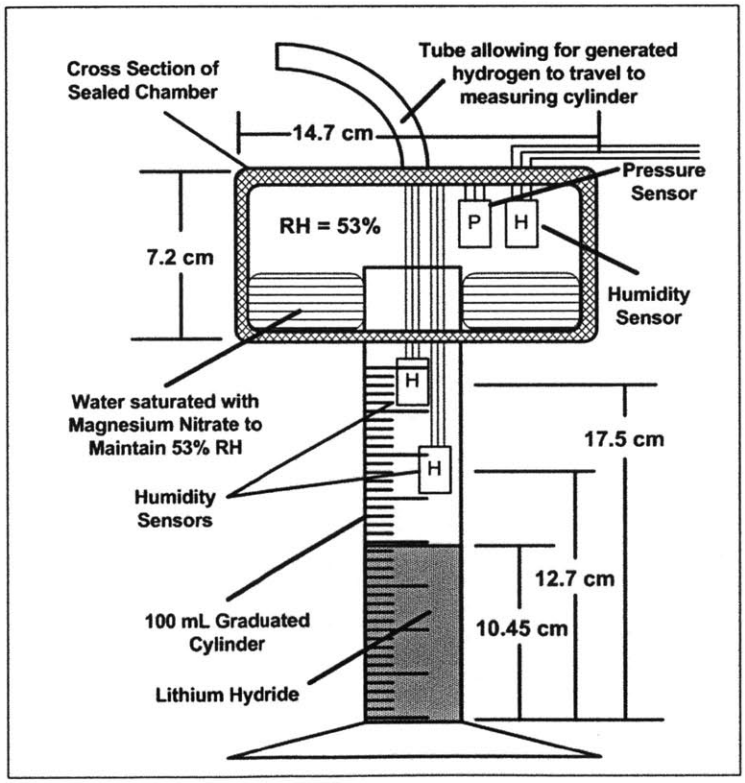

Figure 44: Initial experimental configuration of Experiment B.

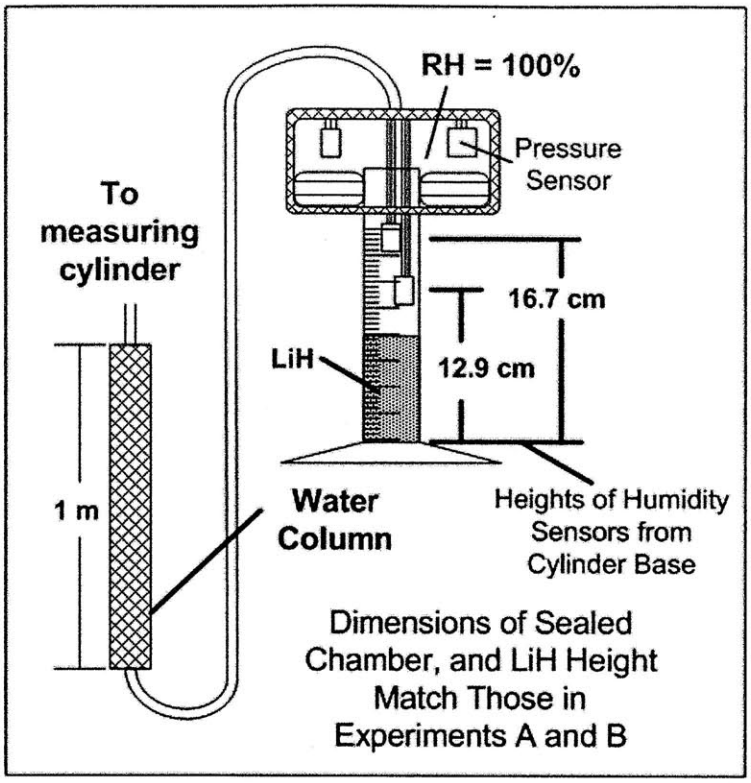

Figure 45: Initial experimental configuration of Experiment C.

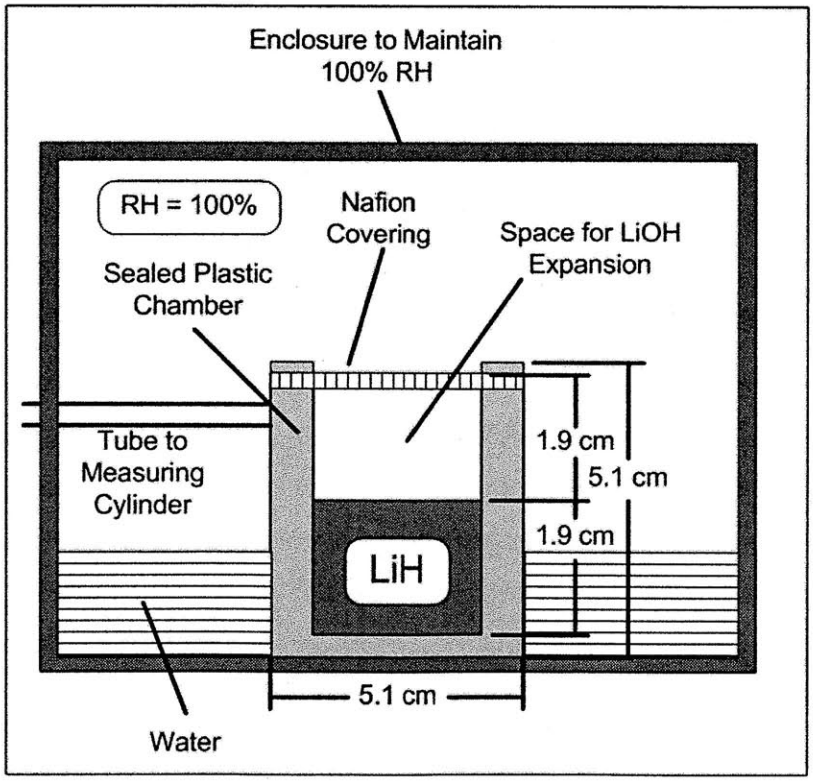

Figure 46: Initial experimental configuration of Experiment D.

6.2 Results of Experiments

Data from the four experiments are presented in the following sections. At the time of writing, these experiments are still being run and the included plots contain the most recent data.

6.2.1 Hydrogen Production Rate

The following four figures depict the rate of hydrogen production as a function of time for each experiment. Figure 47 shows the rate for Experiment A, Figure 48 for Experiment B, Figure 49 for Experiment C, and Figure 50 shows the results for the lithium hydride covered by Nafion, Experiment D.

Two phases of hydrogen production can be seen for all four experiments. The first phase is characterized by an elevated rate of hydrogen production, which lasts from 5-15 days depending on the experiment. After an abrupt drop-off, the second phase is characterized by a much lower rate (about 10-20% the original rate) which slowly falls off.

Although all experiments have rates that are continuously decreasing, the only experiment to have reached zero is the high pressure experiment, Experiment C.

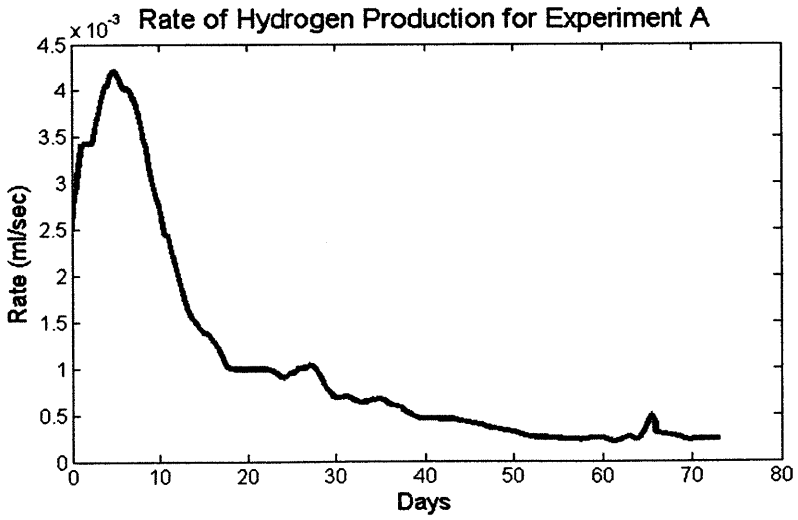

Figure 47: Rate of hydrogen production for Experiment A.

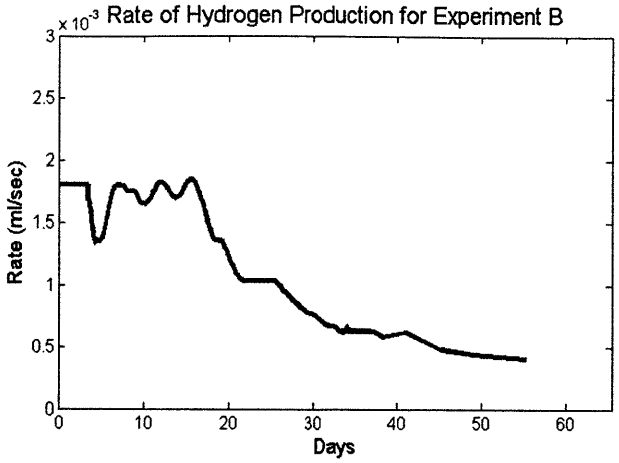

Figure 48: Rate of hydrogen production for Experiment B.

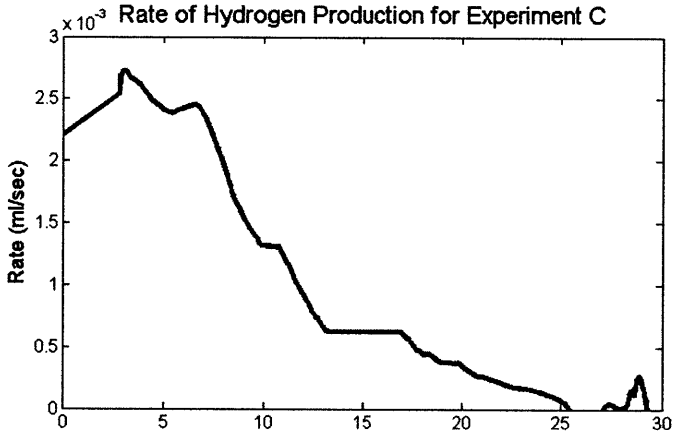

Figure 49: Rate of hydrogen production for Experiment C.

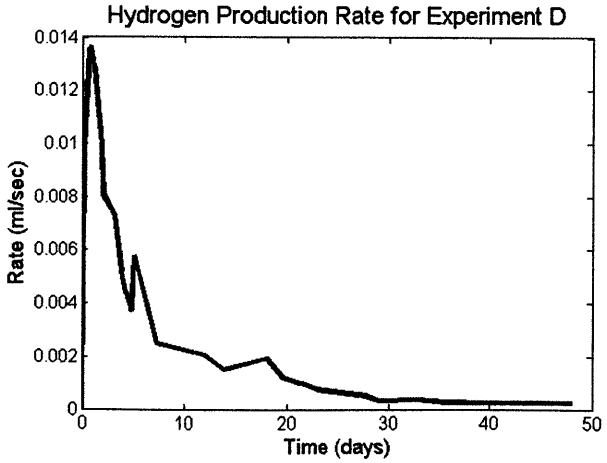

Figure 50: Rate of hydrogen production for Experiment D.

6.2.2 Thickness of Lithium Hydroxide Layer

Figure 51 and Figure 52 show the thickness of the lithium hydroxide layer of the 100% and 53% experiments. In both plots the lithium hydroxide grows rapidly over the first 5-15 days. After this, the layer increases much more slowly. This change in growth rate roughly corresponds to the change in rate of hydrogen production presented in Figures 47 and 48.

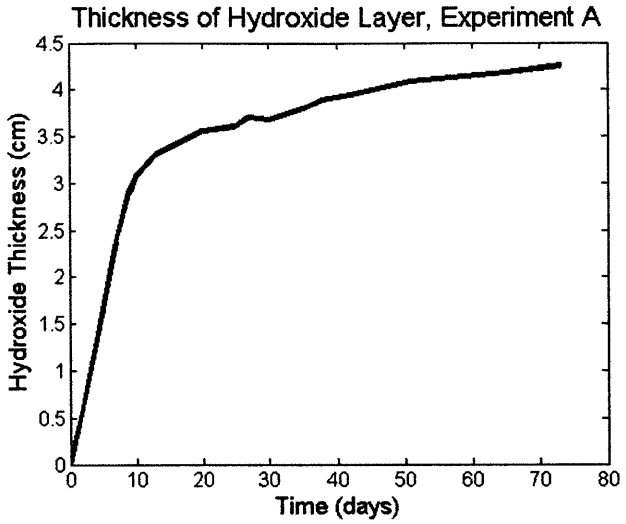

Figure 51: Thickness of lithium hydroxide layer for Experiment A.

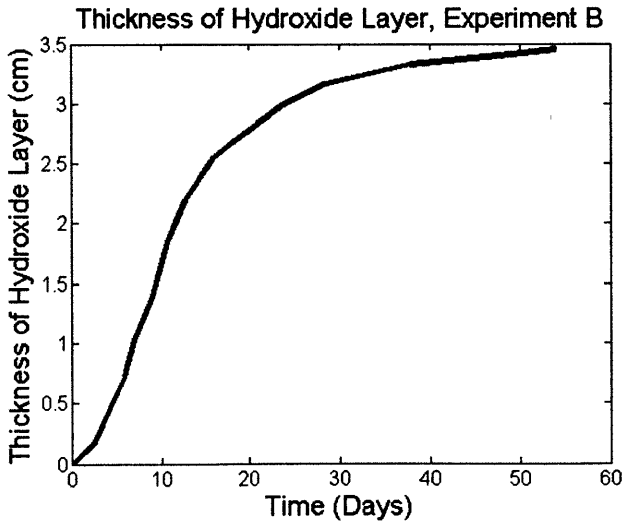

Figure 52: Thickness of lithium hydroxide layer for Experiment B.

6.2.3 Relative Humidity Measurements

Relative humidity sensors are placed at various points of each experiment (refer to Figures 43-45 for exact placement). The data gathered from each of these sensors is plotted in Figures 53-55. In each experiment, the relative humidity along the graduated cylinders rises as a function of time.

In Figure 53 the humidity appears to shoot up toward 100% humidity at approximately 40 days. This is most likely due to humidity sensor failure because the humidity sensors are not designed to be run in high humidities of greater than 90%. In Experiment C, shown in Figure 55, the humidity appears to decrease to zero. This is also most likely due to sensor failure.

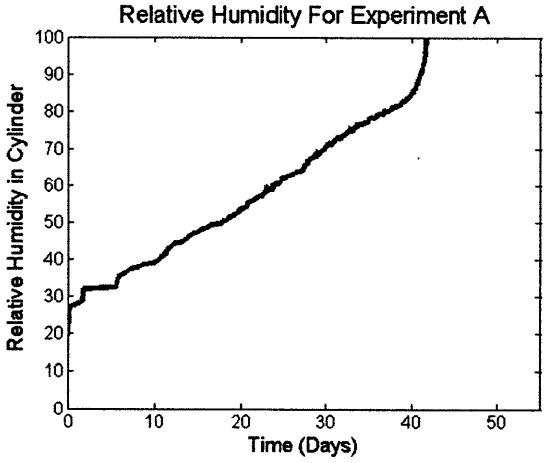

Figure 53: Relative humidity in Experiment A. For position of sensor refer to Figure 43.

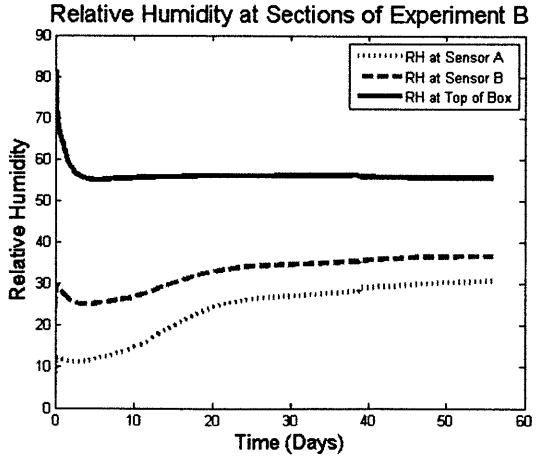

Figure 54: Relative humidity in Experiment B. Sensor A refers to sensor 12.7 cm above base; Sensor B refers to sensor 17.5 cm above base. Refer to Figure 44.

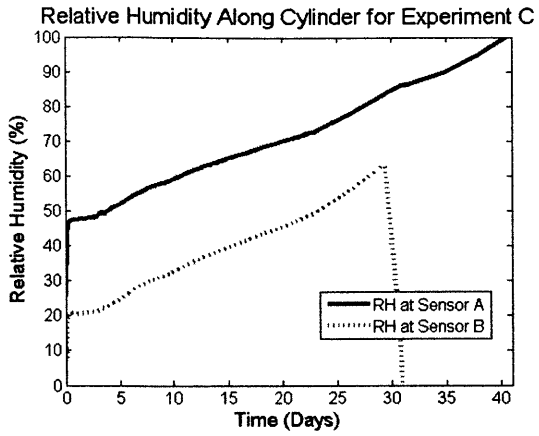

Figure 55: Relative humidity in Experiment C. Sensor B refers to sensor placed 12.9 cm above base. Sensor A refers to sensor placed 16.7 cm above base. Refer to Figure 45.

6.2.1 Volume of Hydrogen Produced

The total volume of hydrogen produced is presented in Figures 56-59. The volumes are the measured variable; the rate plots are derived from these.

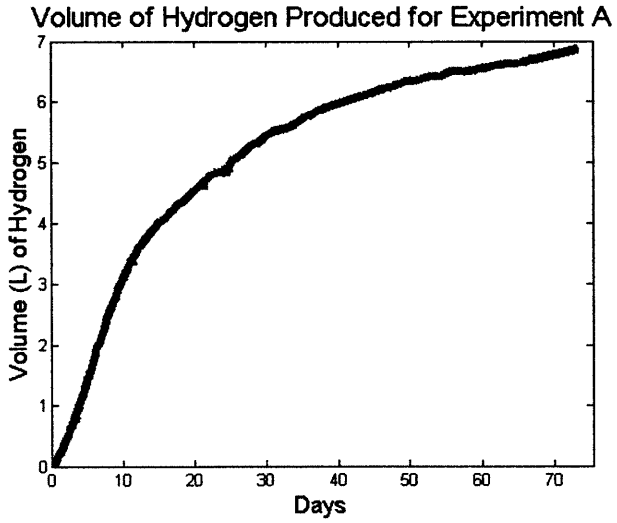

Figure 56: Volume of hydrogen produced for Experiment A.

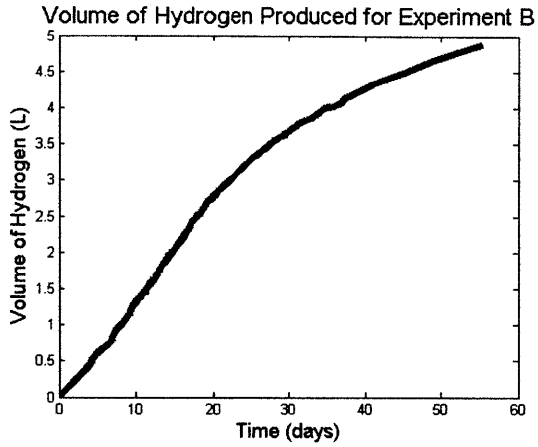

Figure 57: Volume of hydrogen produced for Experiment B.

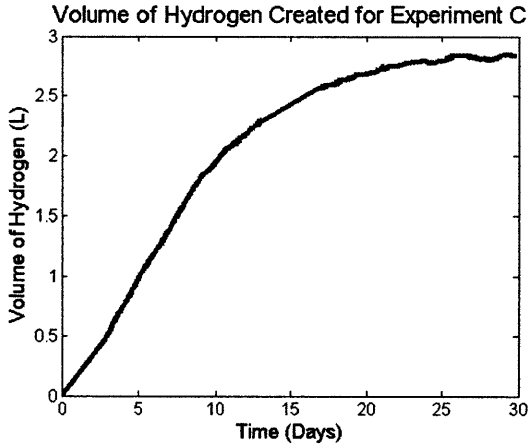

Figure 58: Volume of hydrogen produced for Experiment C.

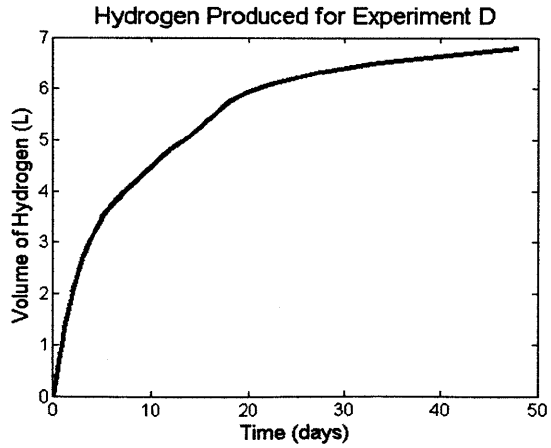

Figure 59: Volume of hydrogen produced for Experiment D.

6.3 Implications of Results for Future Designs

The information in the above plots can be used for future generator designs. For all four experiments, the rate of hydrogen production decreases significantly. Because three of the four experiments are not yet finished at the time of writing, the total hydrogen yield cannot be determined. To make projections about the mass and volume of a future generator, it is assumed that Experiment A does not produce much more than 7 liters of hydrogen. This is reasonable if the rate of hydrogen production continues to drop off. If this were the case, one could expect a hydrogen yield from lithium hydride of 1.3 liters per cm^2 of exposed hydride surface area.

Figure 51 and Figure 52 show that the expansion of the lithium hydroxide layer negatively affects the volumetric efficiency of any lithium hydride generator. As shown in these figures, the hydroxide's volume can expand up to 4 times that of the consumed hydride during the first week of reaction. The rate of rapid expansion does not continue past the first few weeks; after approximately 2-3 weeks, the rate of hydroxide expansion roughly equals the rate that the hydride is being consumed.

One solution to the problem of hydroxide expansion is to constrain it using a sheet of Nafion as done in Experiment 4. Up to the current experimental results, this does not significantly diminish the total volume of hydrogen produced (as seen when comparing the total volume of hydrogen produced for compressed hydroxide versus uncompressed hydroxide, Figure 56 versus Figure 59). Because lithium hydride naturally expands upon conversion to lithium hydroxide even when compressed (1 cm^3 of hydride produces 1.6 cm^3 of hydroxide), an initial gap must be left between the Nafion and hydride to avoid rupturing the Nafion.

Table 9 uses the results of these experiments to calculate the areas and volumes necessary for a hydrogen generator to achieve high utilization efficiency of the lithium hydride. These numbers assume that the hydride is packed in a rectangular bed. They also assume that the fuel cells are 65% efficient. The calculations in Table 9 also assume that Experiment A (which is still producing hydrogen) will stop with a total yield of around 7 liters. Because the experimental results widely differ for the two pressures studied, projections are performed assuming the generator is at atmospheric pressure and at 1.1 bar. The required LiH surface area was calculated by dividing the volume of hydrogen required to produced 250 mW for 3 months (approximately 273 liters) by the total volume of H_2 per cm^2 of hydride (which is determined from the

experiments). The total volume required for hydroxide was calculated based multiplying the volume of hydroxide formed in the experiments by the appropriate factor.

	Total volume (liters) of H_2 per cm^2 of LiH	LiH Surface Area required to power 250 mW PEMFC for 3 months (cm^2)	Volume Required for LiOH (cm^3)	
			Not Compressed	Compressed
Atmospheric Pressure*	1.3	193.0	895.8	499.1
High Pressure (1.1 bar)	0.53	473.4	2145	1092

Table 9: Estimated area and volume of generator using penetration depths from the long-term experiments. *The numbers for the Atmospheric Pressure Case are projections because these experiments have not finished running at the time of writing.

6.4 Conclusions

The experimental results presented in this chapter show that lithium hydride utilization efficiency is a fundamental problem for any hydrogen generator that relies on reacting lithium hydride with water vapor over long periods of time. This is especially an issue for low power, passive devices because there does not appear to be a simple solution to the problem. Even if one were able to increase the reaction rate by separating the hydroxide from the hydride, there is still the problem of expanding lithium hydroxide, which greatly reduces the system's volumetric efficiency.

The best solution may be to accept the problem and find an optimal geometry using the results presented in this chapter. This means that a long life power source based on lithium hydride will require larger surface areas and volumes than otherwise required.

CHAPTER

7

NITROGEN BUILDUP IN DEAD-ENDED ANODE MODE

A feature of fuel cell operation that affects performance and efficiency is the buildup of nitrogen in the fuel cell anode during dead ended anode operation. If the nitrogen is not released, it blocks catalyst reaction cites and chokes the fuel cell in a matter of minutes.

Although this chapter does not relate directly to the development of a lithium hydride generator discussed in chapters 1-6, the results presented form a significant part of the research. Furthermore, any PEM fuel cell system that utilizes the passive generator described above must solve the problem of nitrogen buildup.

7.1 The Problem of Nitrogen Buildup

Many PEM fuel cell anode designs offer two gas ports. One of these ports is always for hydrogen input. The second port is normally placed at a distance from the first port and can either be left open to the atmosphere or closed. If the port is left open, the fuel cell is said to be operating in *blow-through* mode because unused hydrogen is exhausted into the atmosphere. Depending on the fuel cell's operating conditions, the blown-through hydrogen is considerable – up to 90% of the hydrogen input – and operating efficiency is greatly reduced.

To allow the highest hydrogen utilization efficiency, the second port should be closed. This means that no hydrogen is exhausted to the atmosphere and, ideally, all the hydrogen input to the anode will react and produce electricity. This method of PEM fuel cell operation is termed Dead Ended Anode (DEA) operation.

While DEA operation ensures higher hydrogen utilization, it is associated with problems of unwanted nitrogen buildup in the closed anode chamber. Under any operating condition, small

amounts of system gases diffuse across the Nafion membrane; hydrogen, oxygen, water, and nitrogen. Hydrogen and oxygen diffusion are not a problem because they are involved in the chemical reaction. Water diffusion is beneficial to a certain extent because the Nafion membrane must be humidified for proton transport, while large amounts of water diffusion into the closed anode can starve the fuel cell [45].

Diffusion of nitrogen is the chief problem. When the fuel cell operates with air at the cathode instead of pure oxygen (which is true for all of the fuel cells discussed in this study), nitrogen from the air diffuses from the cathode to the anode. Nitrogen does not react with the catalyst and, if not released, builds up in the anode gas channel. The cloud of nitrogen grows and slowly chokes the fuel cell. A point is reached when the fuel cell can no longer maintain the required current and the power output crashes. A PEM fuel cell operating in blow-through mode and dead-ended anode mode is represented in Figure 60 and Figure 61 respectively.

The problem of Nitrogen build-up can be alleviated by purging the anode. If the anode is at a considerable pressure above atmospheric, this is as simple as opening a release valve. The problem is recurrent and, depending on fuel cell operating conditions, the anode will need to be purged once every 5-20 minutes [45].

The valve solution is the accepted solution for this problem in literature and commercially available fuel cells [45]. Two disadvantages of this solution are that it causes wide swings in the anode's hydrogen pressure since the pressure returns to ambient every time the anode is purged and the fact that it requires an actuator, which adds complexity and consumes power. Therefore, for this report, a new method is analyzed, which involves a passive membrane.

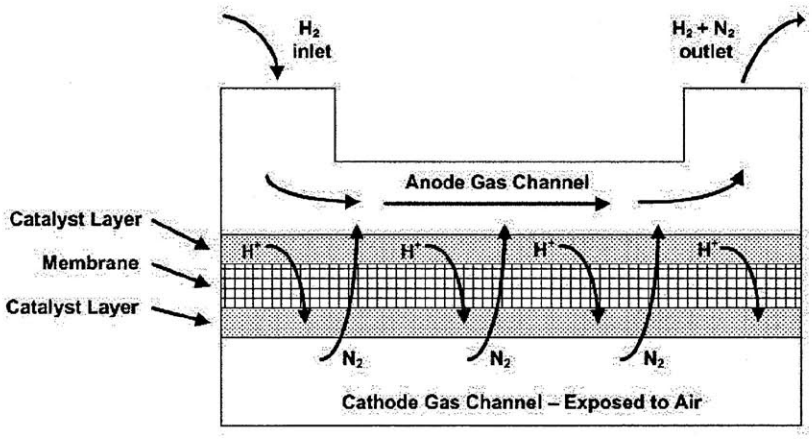

Figure 60: PEM fuel cell operating in flow through mode.

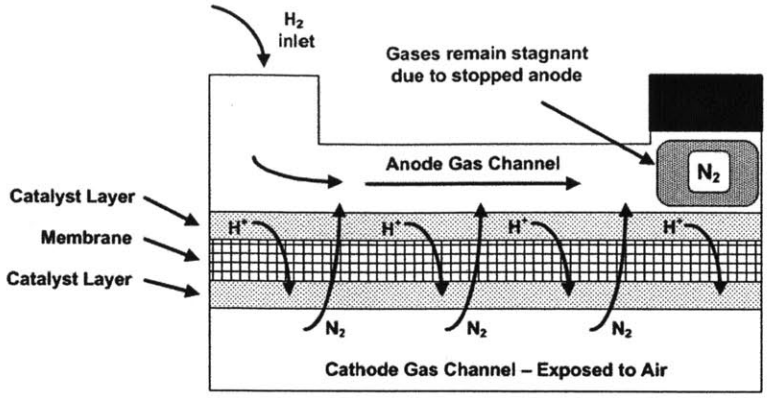

Figure 61: PEM fuel cell operating in Dead-Ended Anode mode.

7.2 Passive Solutions

After having shown that it is possible to purge nitrogen using a pump, passive strategies were employed that relied on the diffusion of nitrogen through membranes. A number of materials were studied until finally settling on layers of polystyrene foam.

7.2.1 Latex Membrane

The first attempt at a passive nitrogen diffuser involved passing the anode's output to a box covered with a latex sheet. The principle of operation was simple and involved a well-known characteristic of latex balloons: once inflated, the balloon will maintain its shape for only a day or two because it slowly allows air to escape into the surroundings. This strategy worked well and allowed sufficient nitrogen to diffuse into the atmosphere so that nitrogen build-up did not affect the fuel cells' performance. An image of the operational nitrogen diffuser is shown in Figure 62, the latex sheet bulges outward because of the significant anode pressure. While this design allowed for nitrogen to diffuse through the latex, its major drawback was mechanical stability. As shown in Figure 63, after prolonged operation the latex ruptured and released the anode pressure.

This initial attempt indicated that passive nitrogen removal was a viable option but a membrane with more mechanical stability would need to be chosen.

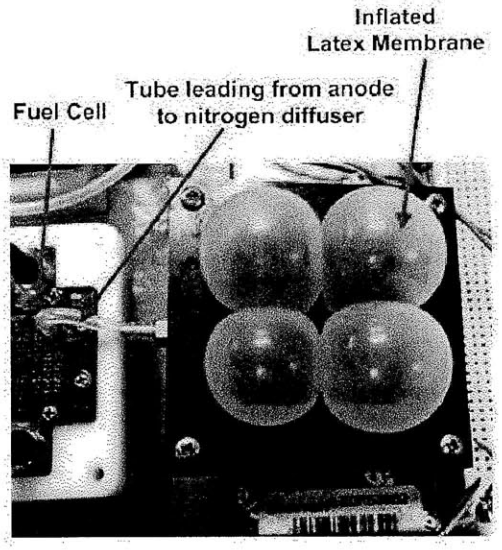

Figure 62: Image of operational latex diffuser.

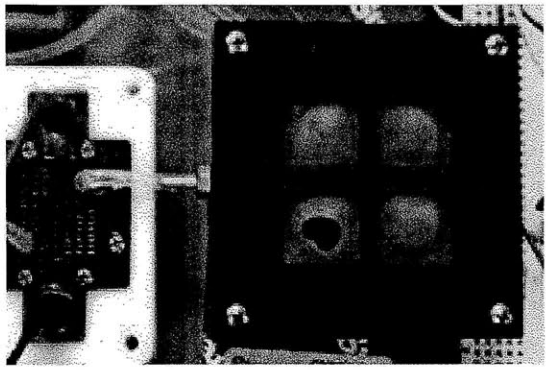

Figure 63: Image of latex diffuser with hole.

7.2.2 Foam Method

After latex, a wide variety of foams (both open cell and closed cell) were purchased in 1/8" – 1/4" sheets and their diffusive properties tested. Certain foams turned out to be too porous to hydrogen (polyethylene) while others did not allow gas to penetrate (EVA foam). Thin sheets of polystyrene foam (similar to the foam found in packaging) turned out to have the desirable amount of flow resistance. A design advantage of using thin layers of polystyrene foam was that the flow resistance could be easily changed by adding or removing layers of foam.

The theory behind both passive methods, i.e. why they should be able to release nitrogen but not release large amounts of hydrogen, is because nitrogen builds up at the end of the fuel cell's anode channel. This is investigated through the development of a model in the next section.

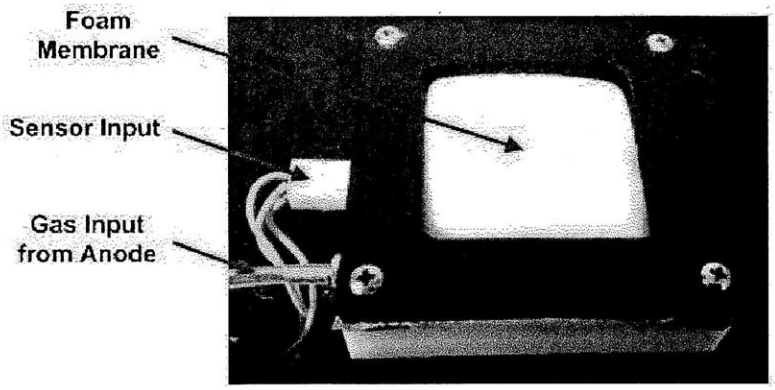

Figure 64: Image of nitrogen release device.

7.3 Model of Passive Nitrogen Removal Subsystem

A model to describe nitrogen accumulation in the anode was developed based on models developed in [46], [45], and [47]. The model is a one-dimensional model of the anode; its geometry and relevant gas flows are presented in Figure 65. Hydrogen enters from the left side and is consumed by the chemical reaction in the x-direction along the channel. It is assumed that the hydrogen is consumed similarly across the x-length of the membrane. This means that there is a non-zero flow velocity from left to right in Figure 65. This is important because it means that the nitrogen that passes from the cathode to the anode is pushed along with the hydrogen and tends to build up in the end of the channel or the portion of the channel furthest from the hydrogen inlet. The model also takes into account oxygen crossover; however, as mentioned above this is not as harmful because oxygen will react at the anode and lead to a small decrease in voltage.

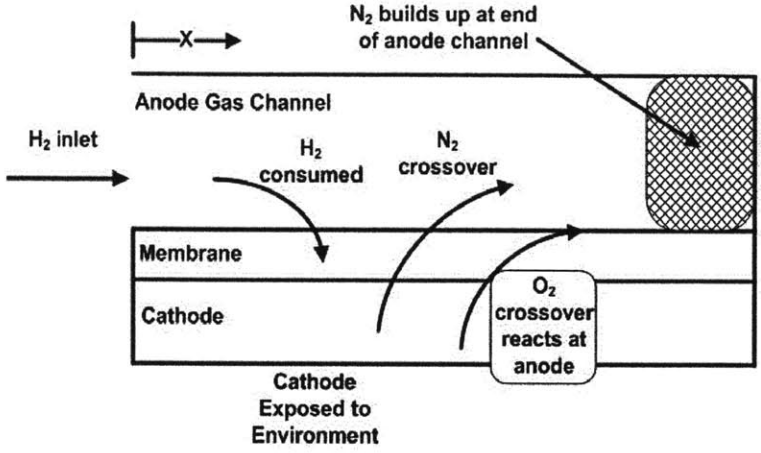

Figure 65: Geometry and mass flows used to model 1D gas crossover.

Each species is modeled by a convection equation for the differential change in mass:

$$\frac{d}{dt}m_i^{An}(x,t) = -\frac{\partial}{\partial x}\left[u(x,t)m_i^{An}(x,t)\right] + \dot{m}_i^{An}(x,t) \qquad (32)$$

where the first term on the right hand side represents the change in mass flow rate with respect to position ($u(x,t)$ represents the flow velocity along the anode) and the second term represents the mass generation term due to gas crossover across the membrane. The i in this equation represents the fact that Eq. (32) represents 3 equations, one for each species involved (N_2, H_2, H_2O). This equation can be written in terms of mole fractions [46],

$$\frac{d}{dt}y_i^{An}(x,t) = -\frac{\partial}{\partial x}\left[u(x,t)y_i^{An}(x,t)\right] + \dot{y}_i^{An}(x,t) \qquad (33)$$

Where $y_{i,an}$ represents the mole fraction of each species in the anode. For each gas, the mass generation term in Eq. (33) can be represented by a separate equation. For hydrogen, this equation takes the form:

$$\dot{y}_{H_2}^{An}(x,t) = -\frac{RT}{p_{An}} \cdot \frac{w_{Ch} + w_R}{w_{Ch} h_{Ch}} \cdot \left(\frac{k_{H_2}}{\delta} y_{H_2}^{An}(x,t) p_{An} + 2\frac{k_{O_2}}{\delta} p_{O_2}^{Ca} + \frac{1}{2F} i_{St}^{App}(t) \right) \quad (34)$$

In this equation, R is the ideal gas constant, T is the anode temperature, w_{ch} is the anode flow channel's width, w_R is the spacing between channels, h_{ch} is the flow channel's height, k_{H2} is the membranes hydrogen permeability, k_{O2} is the membrane's oxygen permeability, p_{An} is the anode's pressure, $p_{O2,ca}$ is the oxygen partial pressure at the cathode δ is the membrane's thickness, F is Faraday's constant, and i_{app} is the fuel cell's current. The values of these constants are given in Appendix C. The three components of Equation (34) can be broken down: the first term represents hydrogen that permeates from the anode to the cathode, the second term represents hydrogen that reacts at the anode with oxygen that has permeated from the cathode to the anode, and the third term represents hydrogen that reacts to produce electricity. Because of this, the third term is linearly dependent on current. Similarly, the equation for nitrogen generated takes the form:

$$\dot{y}_{N_2}(x,t) = \frac{RT}{p_{An}} \cdot \frac{w_{Ch} + w_R}{w_{Ch} h_{Ch}} \cdot \frac{k_{N_2}}{\delta} \left(p_{N_2}^{Ca} - y_{N_2}^{An}(x,t) p_{An} \right) \quad (35)$$

The only new constants are k_{N2} which is the membrane's permeability to nitrogen, and $p_{N2,ca}$ which is the partial pressure of nitrogen at the cathode. The first term on the right hand side in parenthesis in Eq. (35) represents nitrogen that permeates from the cathode to the anode and the second term represents the potential for nitrogen to permeate back across the membrane from the anode to the cathode. Finally, the term for water generation at the anode is

$$\dot{y}_{H_2O}(x,t) = y_{H_2O}^{An} \cdot \frac{\partial}{\partial x} u(x,t) \quad (36)$$

where y_{H2O} is the mole fraction of water at the anode and is assumed constant:

$$y_{H_2O}^{An} = \frac{\varphi_{An} P_{Sat}(T)}{p_{An}} \quad (37)$$

Another constraint on this system of three partial differential equations (one for N_2, H_2, H_2O) is that all mole fractions must add up to 1:

$$\sum_i \frac{d}{dt} y_i^{An}(x,t) = -\sum \frac{\partial}{\partial x}\left[u(x,t) y_i^{An}(x,t)\right] + \sum_i \dot{y}_i^{An}(x,t) = 0 \tag{38}$$

Finally, initial conditions and boundary conditions are required to solve this system. It is assumed that there is no nitrogen in the anode channel to begin, that is:

$$y_{N_2}(x,0) = 0 \tag{39}$$

and the initial mole fraction of water in the anode channel is set at a constant:

$$y_{H_2O}(x,0) = \frac{\varphi_{An} P_{Sat}(T)}{p_{An}} \tag{40}$$

Since all mole fractions must add to one, this means that the initial mole fraction of hydrogen is:

$$y_{H_2}(x,0) = 1 - \frac{\varphi_{An} P_{Sat}(T)}{p_{An}} \tag{41}$$

Like initial conditions, it is assumed that there is no nitrogen in the incoming hydrogen stream:

$$y_{N_2}(0,t) = 0 \tag{42}$$

$$y_{H_2}(x,0) = 1 - \frac{\varphi_{An} P_{Sat}(T)}{p_{An}} \tag{43}$$

The difference between the model developed in this report and the model developed in [47], [45], and [46] is the velocity boundary condition at the channel's end. A fuel cell operating in DEA mode assumes that there is zero velocity at the channel's exit because it is stopped. This report assumes that there is a non-zero flow velocity due to the permeation of gas across the nitrogen diffuser. This boundary condition is given as:

$$u(L,t) = \frac{\kappa}{\mu} \frac{\Delta P}{\Delta x} \tag{44}$$

where L represents the length of the anode channel, κ the foam's permeability, μ the fluid dynamic viscosity, and $\Delta P/\Delta x$ the pressure gradient over the foam's depth.

To take into account the effect of nitrogen accumulation on the fuel cell's performance, the change in the fuel cell's effective area must be modeled. As a function of total current, the current density is given by:

$$i_{St}^{App}(t) = \frac{I_{St}}{A_{effective}(t)} \tag{45}$$

where the effective area, $A_{effective}(t)$, is the membrane area not clogged by the nitrogen buildup and still able to produce power. This is based on the length of the 1-dimensional channel where there is still considerable hydrogen present:

$$A_{effective}(t) = n_{Ch}(w_{Ch} + w_R)L_{effective}(t) \tag{46}$$

where n_{ch} are the number of channels and $L_{effective}$ is the length of the channel where the hydrogen mole fraction is above a certain threshold that resembles choking. This is the length that still produces power,

$$L_{effective}(t) = x \mid y_{H_2}(x,t) > y_{H_2,choking} \tag{47}$$

These equations were simulated with parameters matching the Horizon fuel cells available to this research. In Figure 66, the results of the simulation are compared with experimental results running a fuel cell system. These results are for a fuel cell operating in dead ended anode mode at a very low power (~20 milliwatts). After approximately 25 minutes, the voltage rapidly decreases due to nitrogen buildup. As shown in Figure 66, there is error between the model and the experimental results. One reason for this is that the model uses a 1-dimensional anode flow model, while the Horizon fuel cells should be modeled with at least 2 dimensions.

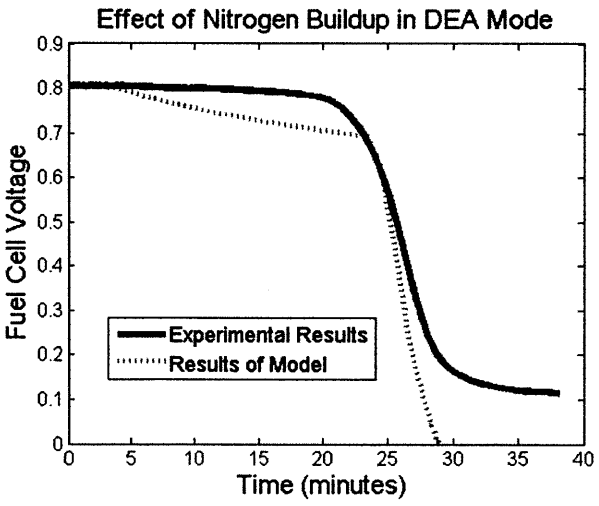

Figure 66: Voltage decrease of fuel cell operating at 20 mW due to nitrogen buildup.

The main change to the model developed in literature for dead-ended anode operation is the boundary condition on velocity at the anode's exit. Instead of being zero, the flow velocity can be related to the foam's permeability, the gas's viscosity, and the pressure gradient through the following equation:

$$V_{exit} = \frac{\kappa}{\mu}\frac{\Delta P}{\Delta x} \tag{48}$$

where V_{exit} is the flow velocity at the anode's exit (m/s), κ is the foam's permeability to the gas of interest (m^2) , μ is the gas's dynamic viscosity (Pa*s), ΔP is the pressure difference between the anode exit and environment (Pa), and Δx is the foam's thickness. The permeability of the polystyrene foam, κ, was determined experimentally for hydrogen and air (which is assumed to approximate nitrogen). For hydrogen the permeability was determined to be 1.8e-14 m^2 and for air the permeability was 6.9e-15 m^2. The model was simulated with this boundary condition (which assumes the passive foam nitrogen diffuser is being used). A plot of the model's predicted voltage is compared against the experimentally observed voltage in Figure 67 , both cases running a fuel cell at approximately 20 mW. The plot is uneventful as neither voltage changes much in time.

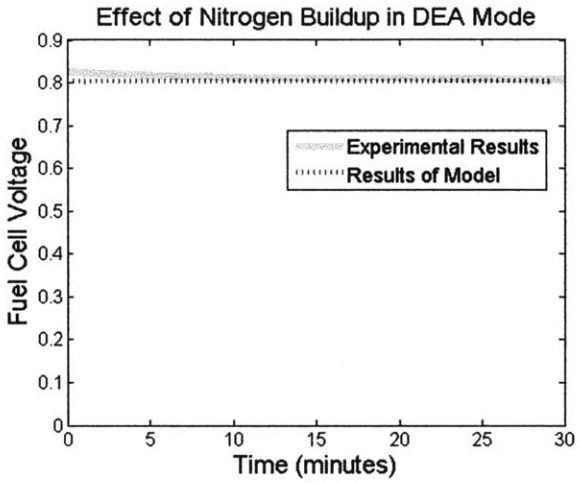

Figure 67: Voltage of fuel cell with foam membrane attached to anode.

The model also predicts the mole fractions of hydrogen and nitrogen as a function of distance along the anode channel. These results are presented in Figure 68 and Figure 69. From these graphs, it is evident that even with the foam membrane attached to the fuel cell, nitrogen still builds up toward the end of the anode. In spite of this, enough hydrogen is still present to avoid hydrogen starvation.

While using foam is simpler than employing valves and pumps to release the nitrogen, the question remains whether it is more efficient. A certain amount of hydrogen is lost through the foam and can be predicted from the model using the equation:

$$n_{H_2,lost} = \frac{y_{H_2} u A_{an} P_{an}}{RT} \tag{49}$$

Where n represents the moles of hydrogen lost to the atmosphere, y is the mole fraction of hydrogen, u is the velocity, A_{an} is the anode's cross-sectional area, P_{an} is the anode's pressure, R is the ideal gas constant, and T is the temperature. Both the mole fraction of hydrogen and the velocity are taken at $x=L$, the end of the anode. This calculation yields an efficiency of 82% for the fuel cell operating at 1.1 bar, which means that 18% of the system hydrogen is lost through the nitrogen diffuser. Due to lack of a hydrogen detector, this study was not able to experimentally validate this number.

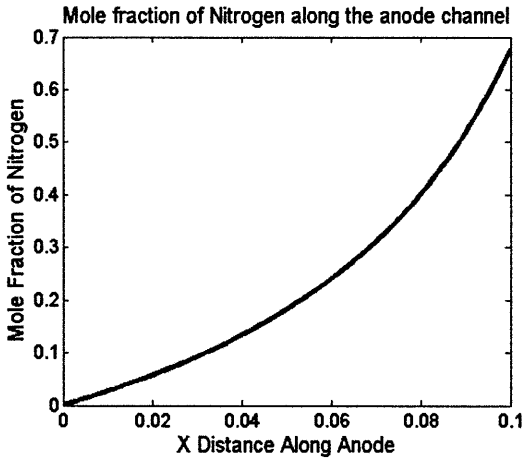

Figure 69: Mole fraction of nitrogen along the 1-dimensional anode channel for system with foam release.

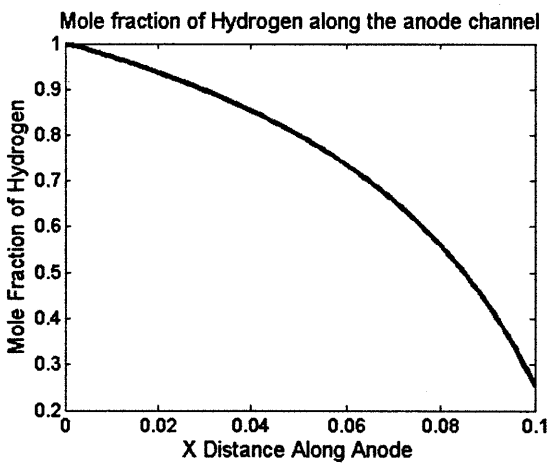

Figure 68: Mole fraction of hydrogen along 1-dimensional anode channel for system with foam release.

This study develops a passive nitrogen removal device to operate the fuel cell system in dead end anode mode. The passive device is operated on the theory that nitrogen builds up at the end of the anode channel. Therefore, it should be possible to create a device that allows sufficient nitrogen to exit the system while minimizing the hydrogen loss. Using the model from literature and expanded on in this chapter, the thickness of the polystyrene foam can be optimized to meet these criteria.

CHAPTER

8

CONCLUSIONS AND FUTURE WORK

8.1 Summary of Results

This thesis developed and experimentally tested a hydrogen generator for low-power PEM fuel cells using lithium hydride as the hydrogen source. Lithium hydride was considered the fuel of choice because of its high hydrogen content and the ease with which one is able to control the reaction.

A number of actively controlled generator designs were considered that relied on pumps and servo motors to control the pressure of the produced hydrogen. One drawback to these designs was their complexity, so a passive system was designed based on a compliant valve mechanism to regulate the pressure. This design was modeled and tested successfully over the short-term.

After running short-term experiments, a 3 month benchtop fuel cell experiment was designed and run. The system ran for two months before suffering from hydrogen starvation. The starvation was due to a buildup of the byproduct lithium hydroxide. While it was originally assumed that hydroxide formation would not prevent water vapor from reaching the hydride, this assumption was false over the long-term.

The final part of the research studied the long-term behavior of lithium hydride hydrolysis. A series of experiments were run that determined that the rate of hydrogen production does significantly decrease after the first 2-3 weeks of reaction. Estimates of the maximum volume per surface area of hydrogen were obtained that will help the design of future generators.

8.2 Future Work

The most immediate extension of this work is to use the models developed and the long-term experimental results to design and experimentally validate an optimized lithium hydride generator. The short-term mathematical model developed in Chapter 4 can help design the passive valve for control of the pressure and data from the long-term experiments presented in Chapter 7 can aid determining the maximum penetration depth of water vapor into the hydride bed.

The passive nitrogen removal subsystem discussed in Chapter 8 can also be optimized. Using the model discussed in Chapter 8, the thickness of the polystyrene membrane could be optimized to minimize hydrogen leakage while ensuring adequate removal of nitrogen.

Although out of the scope of this thesis, one question that future work may investigate is whether the design discussed in this thesis is scalable to higher powers. This is a non-trivial design challenge because hydrogen production rate scales with surface area of the hydride exposed to water vapor. One can imagine many geometries that maximize surface area while reducing system volume (such as casting grooves in the hydride or suspending the hydride in a mesh), but many of these ideas suffer from the expansion of lithium hydroxide choking the source of water vapor. It would be better to develop an active control system that reacts hydride with liquid water and employs active mechanisms to remove the byproduct lithium hydroxide.

References

[1] Shad Roundy, Dan Steingart, Luc Frechette, Paul Wright, and Jan Rabaey, "Power Sources for Wireless Sensor Networks," in *Wireless Sensor Networks*, Karl Holger and Adam Wolisz, Eds. Berlin, Germany: Springer Verlag, 2004, ch. 1, pp. 1-17.

[2] Su W Sankasubramanium, Y. Cayirci, and E. Akyildiz, "A Survey of Sensor Networks," *IEEE Communications Magazine*, pp. 102-114, August 2002.

[3] G. Ritchie, "Recent Developments and Likely Advances in Lithium Rechargeable Batteries," *Journal of Power Sources*, vol. 136, no. 2, pp. 285-289, 2006.

[4] J.M. Tarascon and M. Armand, "Issues and challenges facing rechargeable lithium batteries," *Nature*, vol. 414, pp. 359-367, 2004.

[5] J Thangavelautham and S. Dubowsky, "On the Catalytic Degradation in Fuel Cell Power Supplies for Long Life Mobile Field Sensors," *Under Review in Journal of Fuel Cells*, pp. 1-42, 2012.

[6] I. Uehara, T. Sakai, and H. Ishikawa, "The state of research and development for applications of metal hydrides in Japan," *Journal of Alloys and Compounds*, vol. 253-254, pp. 635-641, 1997.

[7] Billur Sakintunaa, Farida Lamari-Darkrim, and Michael Hirscher, "Metal hydride materials for solid hydrogen storage: A review," *International Journal of Hydrogen Energy*, vol. 32, pp. 1121-1140, 2007.

[8] Daniele Gallardo, "Power Management for Micro PEM Fuel Cells," Politecnico di Torino, Turin, Thesis 2010.

[9] U.S. Department of Energy. (2011, March) Types of Fuel Cells. [Online]. http://www1.eere.energy.gov/hydrogenandfuelcells/fuelcells/fc_types.html

[10] F. Barbir, *Fuel Cells: Theory and Practice*. Burlington, USA: Academic Press, 2005.

[11] Smithsonian Institution. (2004, January) PEM Fuel Cell History. [Online]. http://americanhistory.si.edu/fuelcells/pem/pemmain.htm

[12] Louis Schlapbach and Andreas Zuettel, "Hydrogen-storage materials for mobile applications," *Nature*, vol. 414, pp. 353-358, November 2001.

[13] J.O. Bockris, *Energy: the solar - hydrogen alternative*. New York, USA: John Wiley and Sons Inc., 1975.

[14] U.S. Department of Energy. (2001, December) Hydrogen Fuel Cell Engines, Module 1: Hydrogen Properties. Document. [Online]. http://www1.eere.energy.gov/hydrogenandfuelcells/tech_validation/pdfs/fcm01r0.pdf

[15] U.S. Department of Energy. (2010, November) Fuel Cells Technology Program: Production. Document. [Online]. http://www1.eere.energy.gov/hydrogenandfuelcells/pdfs/doe_h2_production.pdf

[16] D. Chandra, "Intermetallics for Hydrogen Storage," in *Solid State Hydrogen Storage: Materials and Chemistry*, Gavin Walker, Ed. Cambridge, United Kingdom: Woodhead Publishing Limited, 2008, ch. 12, pp. 317-324.

[17] Z.T. Xia and S.H. Chan, "Feasibility study of hydrogen generation from sodium borohydride solution for micro fuel cell applications," *Journal of Power Sources*, vol. 152,

pp. 46-49, 2005.

[18] W.D. Machin and F.C. Tompkins, "Kinetics of the Reaction of Water Vapor with Crystalline Lithum Hydride," *Transactions of the Faraday Society*, vol. 62, pp. 2205-2218, 1966.

[19] Governmental Affairs Institute Washington DC Research Division, "30-Watt Lithium Hydride Fuel Cell," US Army Electronics Command, Washington DC, Government Document AD0840361, 1968.

[20] Gerald K. Pitcher, "Solid Lithium Hydride as a Hydrogen Source for Fuel Cells," Naval Undersea Warfare Center Division Newport , Newport, 1996.

[21] Andrew W. McClaine and et. al., "Hydrogen Transmission with Metal Hydride-Organic Slurry and Advanced Chemical Hydride/Hydrogen for PEMFC Vehicles," Thermo Technologies, Proceedings of the 2000 U.S. DOE Hydrogen Program Review 2000.

[22] Michael T. Kelly, *Fuel Cells and Hydrogen Storage*, Andrew Bocarsly and D. Michael P. Mingos, Eds. Berlin, Germany: Springer-Verlag, 2011.

[23] Gerald P. Lahti, "Fission Neutron Attenuation in Lithium-6, Natural Lithium, and Tungsten," National Aeronautics and Space Administration, Cleveland , NASA Technical Note NASA TN-4684, 1968.

[24] Public Broadcasting Service. (2009) American Experience. [Online]. http://www.pbs.org/wgbh/amex/bomb/peopleevents/pandeAMEX60.html

[25] C. Haertling, R.J. Hanrahan Jr., and R. Smith, "A literature review of reactions and kinetics of lithium hydride hydrolysis," *Journal of Nuclear Materials*, vol. 349, pp. 195-233, 2006.

[26] V.C.Y. Kong, D.W. Kirk, F.R. Foulkes, and J.T. Hinatsu, "Development of hydrogen storage for fuel cell generators II: utilization of calcium hydride and lithium hydride," *International Journal of Hydrogen Energy*, vol. 28, pp. 205-214, 2003.

[27] Douglas A. Broughton, "Hydrolysis of Lithium Hydride," University of Reading, Reading, Doctoral Thesis in the Department of Chemistry 2001.

[28] Daniel M. Boryta and Albert J. Maas, "Factors Influencing the Rate of Carbon Dioxide Reaction with Lithium Hydroxide," *Industrial & Engineering Chemistry Process Design and Development*, vol. 10, no. 4, pp. 489-494, October 1971.

[29] Carol L. Haertling, Robert J. Hanrahan Jr., and Joseph R. Tesmer, "Hydrolysis Studies of Polycrystalline Lithium Hydride," *Journal of Physical Chemistry*, vol. 111, pp. 1716-1724, January 2007.

[30] M. Balooch, L.N. Dinh, and D.F. Calef, "The reaction kinetics of lithium salt with water vapor," *Journal of Nuclear Materials*, vol. 303, pp. 200-209, 2002.

[31] FMC Corporation, "Lithium Hydroxide Monohydrate Technical Grade," FMC Corporation, Charlotte, Datasheet CAS No.1310-66-3, 2007.

[32] L.N. Dinh and M.A. Schildbach, "Hydrogen Outgassing from Lithium Hydride," in *Nuclear Materials Research Development*, Joel E. Keister, Ed. Hauppauge , United States of America: Nova Publishers, 2007, ch. 6, pp. 257-283.

[33] Jonathan Phillips and Michael C. Bradford, "A Calorimetric Study of the Mechanism and Thermodynamics of the Lithium Hydride-Water Reaction at Elevated Temperatures," *Energy & Fuels*, vol. 9, no. 4, pp. 569-573, July/August 1995.

[34] Kennard V. Wilson, Brian M. Patterson, and Jonathan Phillips, "Microbalance study of the

corrosion kinetics of lithium hydride by water," *Journal of Nuclear Materials*, vol. 374, pp. 229-240, August 2008.

[35] Grigorii L. Soloveichik, "Metal Borohydrides as Hydrogen Storage Materials," *Material Matters*, vol. 2.2, no. 11, 2007.

[36] D.W. Oxtoby, H.P. Gillis, and A Campion, *Principles of Modern Chemistry*, 6th ed. Belmont, USA: Brooks/Cole, 2007.

[37] L. Greenspan, "Humidity Fixed Points of Binary Saturated Aqueous Solutions," *Journal of Research of the National Bureau of Standards*, pp. 89-96, 1977.

[38] Dolomite Corporation. (2011, May) Syringe Pumps. [Online]. http://www.dolomite-microfluidics.com/webshop/pumps-syringe-pumps-c-38_46

[39] Epson Corporation. (2011, May) Micro Piezo Technology. [Online]. http://global.epson.com/innovation/micro_piezo/index.html

[40] Takasago Electric Inc. (2011, May) Piezoelectric Micro Pump. [Online]. http://www.takasago-elec.com/products_pump/piezo/

[41] Ryan P. O'Hayre, Suk-Won Cha, Whitney Colella, and Fritz B. Prinz, *Fuel Cell Fundamentals*. Hoboken, United States of America: John Wiley & Sons, 2006.

[42] Sathya Motupally, Aaron J. Becker, and John W. Weidner, "Diffusion of Water in Nafion 115 Membranes," *Journal of Electrochemical Society*, vol. 147, no. 9, pp. 3171-3177, April 2000.

[43] Vadim Khayms, *Linear Algebra and Partial Differential Equations for Engineers*. Stanford, CA: Stanford Course Reader, 2010.

[44] I Muller and P. Strehlow, *Rubber and Rubber Balloons, Paradigms of Thermodynamics*. Berlin-Heidelberg, Germany: Springer-Verlag, 2004.

[45] Jason B. Siegel, Stanislav V. Bohac, Anna G. Stefanopoulou, and Serhat Yesilyurt, "Nitrogen Front Evolution in Purged Polymer Electrolyte Membrane Fuel Cell with Dead-Ended Anode," *Journal of Electrochemical Society*, vol. 157, no. 7, pp. 1081-1093, May 2010.

[46] Eric A. Mueller, Florian Kolb, Lino Guzzella, Anna Sefanopoulou, and Denise A. McKay, "Correlating Nitrogen Accumulation With Temporal Fuel Cell Performance," *Journal of Fuel Cell Science and Technology*, vol. 7, April 2010.

[47] Shyam S. Kocha, J. Deliang Yang, and Jung S. Yi, "Characterization of Gas Crossover and Its Implications in PEM Fuel Cells," *AlChE Journal*, vol. 52, no. 5, February 2006.

[48] V.C.Y. Kong, F.R. Foulkes, D.W. Kirk, and J.T. Hinatsu, "Development of hydrogen storage for fuel cell generators. I Hydrogen generation using hydrolysis hydrides," *International Journal of Hydrogen Energy*, vol. 24, pp. 665-675, 1999.

[49] C.E. Holcombe, "Retardation of the Reaction of Lithium Hydride with Water Vapor," Union Carbide Corporation - Nuclear Division, Oak Ridge Y-12 Plant, Tennessee, Y-1835, 1972.

[50] Sathya Motupally, Aaron J. Becker, and John W. Weidnera, "Diffusion of Water in Nafion 115 Membranes," *Journal of The Electrochemical Society*, vol. 147, pp. 3171-3177, 2000.

[51] John Crank, *The Mathematics of Diffusion*, 2nd ed. London, Great Britain: Oxford University Press, 1975.

[52] J. Tanski, "Analysis of a New Reaction Mechanism for Hydrolysis of LiH," Los Alamos National Laboratory, LAUR-00-5324, 2000.

[53] Thomas Roy Crompton, *Battery Reference Book*, 3rd ed. Oxford, Great Britain: Reed Educational and Professional Publishing, 2000.

[54] S.R. Narayan and Thomas Valdez, "High Energy Portable Fuel Cell Power Sources," *The Electrochemical Society Interface*, pp. 40-45, Winter 2008.

[55] Protonex Technology Corporation. (2009) Protonex. [Online]. http://www.protonex.com/downloads/products/Protonex_UAV_Spec_Sheet.pdf

[56] I. Su W., Sankasubramanium, Y., Cayirci, E. Akyildiz, "A Survey of Sensor Networks," *IEEE Communications Magazine*, pp. 102-114, August 2002.

[57] Kavya Manyapu, "Feasibility Study of Long-Life Micro Fuel Cell Power Supply for Sensor Networks for Space and Terrestrial Applications," MIT, Cambridge, SM Thesis 009-25, 2010, 2010.

APPENDIX

A

VOLUME MEASUREMENT TECHNIQUE

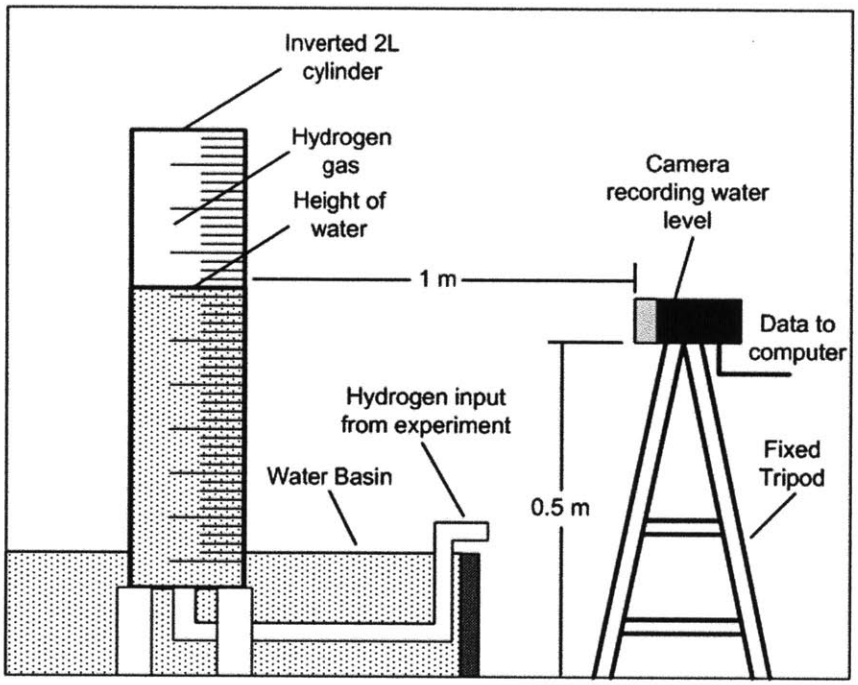

Figure 70: Method of Measuring Hydrogen Gas Output.

Measurement of the hydrogen output volume was important for a number of experiments in this thesis. The volume was measured by inverting a graduated cylinder in a pan of water so that the cylinder was filled with water. A tube was inserted at the bottom of the cylinder that carried hydrogen from the experiment into the cylinder. When using this method, the difference in pressure between the cylinder's bottom and the height of the hydrogen gas must be accounted for to accurately measure hydrogen volume.

Two methods were used to measure the hydrogen that collected in the cylinder. The first and simplest method employed involved observing and recording the volume of hydrogen generated. Because many experiments were carried out over weeks or months, it was not practical to continuously monitor the experiments. For this reason, a second method was developed that relied on a video camera detecting the water level in the cylinder and a computer recording the volume of hydrogen generated. This is shown in Figure 70. While there are many methods to sense and record water level, this method was chosen because of cost and accuracy.

A number of techniques were used to make the video capture technique more accurate and reduce fluctuations. Applying a Laplacian of Gaussian (LoG) filter before processing the captured image worked well to stabilize readings and reduce error. This filter can be easily applied in Matlab. Coloring the water blue with food coloring and placing the cylinder against a white background made the water level much easier to find. Bright red tape was placed along the cylinder so that the program could find the water level in relation to known markers and calculate the volume accordingly.

APPENDIX

B

INVERTED HYDRIDE EXPERIMENT

The problem of the lithium hydride hydrolysis reaction clogging up over longer time periods (1-3 months) is detailed in Chapter 6. Although this research did not have time to fully explore designs that solve this problem, one design was attempted. This design held the lithium hydride upside down under the hypothesis that the lithium hydroxide would fall away and leave the lithium hydride surface free to react with water vapor. The rate of hydrogen production was measured using this approach and it was determined that it suffers from the same problems as the non-inverted reaction chambers.

B.1 Experimental Design

The inverted hydride experiment was setup as depicted in Figure 71. Lithium hydride powder was compressed into a cylindrical pocket that had been milled in acrylic plastic. A coarse metal mesh was placed on top the lithium hydride to prevent the hydride from falling. A Nafion membrane was wrapped around the device to allow water vapor to enter from the environment.

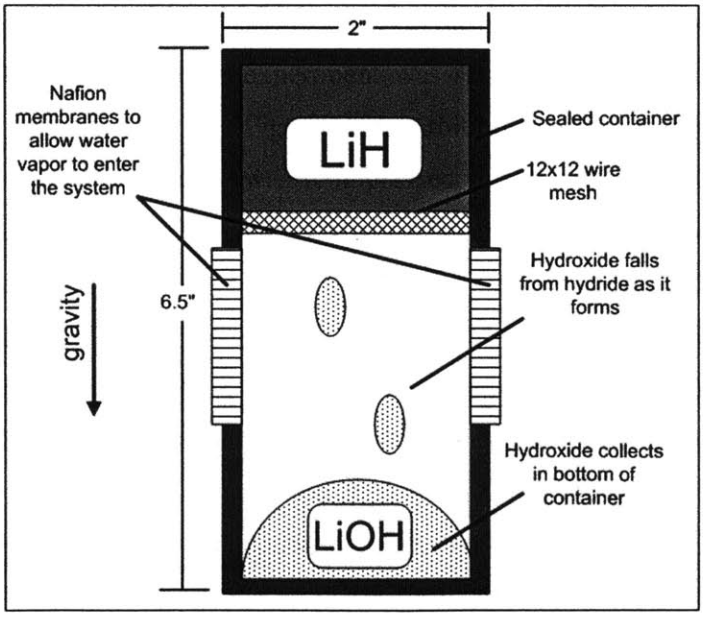

Figure 71: Setup for inverted hydride experiment.

This experiment was designed to allow the lithium hydroxide to fall

freely from the lithium hydride surface upon hydrolysis. This would prevent lithium hydroxide from clogging the reaction and prevent the rate of hydrogen production from decreasing. This would not solve the problem of lithium hydroxide expansion; the lithium hydroxide would still build up in the bottom of the container.

B.2 Results and Conclusions

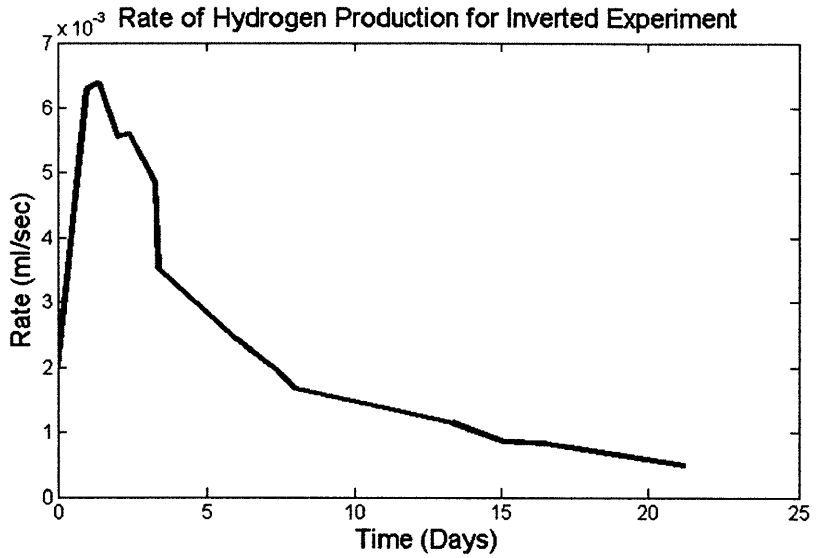

Figure 72: Rate of hydrogen production for inverted hydride experiment.

The rate of hydrogen production over the first three weeks of the inverted experiment are presented in Figure 72. The rate looks similar to the rate plots presented in Chapter 6. There is an initial period of high hydrogen production, which is followed by a sharp decrease between days 5-10, and finally reduced rate that slowly decreases. The reason for this is because the idea behind the experiment (that lithium hydroxide will fall from the hydride surface) is not true. Hydroxide only fell from the hydride for the first week; after this, the hydroxide clung to the hydride surface and formed a dense solid between the metal mesh and lithium hydride surface.

From Figure 72, one can conclude that inverting the hydride does not significantly improve the rate of hydrogen production over time. While it may be possible to consider other geometries or passive mechanisms that solve the problem of hydroxide buildup, this is a non-trivial design task.

APPENDIX

C

PARAMETERS USED IN SIMULATIONS

Constant	Variable	Value	Units
Generator Geometry			
Depth of hydride bed	N/A	0.01	m
Surface area of LiH	N/A	0.012	m^2
Volume of generator headspace	N/A	0.0006	m^3
Height of gap between Nafion and latex	N/A	0.0127	m
Nafion surface area	N/A	0.0117	m^2
Nafion Properties			
Density of Nafion	P	2	g/cm^2
Molar mass of Nafion	M_{Nafion}	1100	g/mol
Nafion Thickness	t_{Nafion}	0.0178	m
Physical Properties			
Density of Water	ρ	1000	kg/m^3
Molar mass of water	M_{H2O}	18	g/mol
Water saturation pressure	P_{sat}	2338	Pa
Ideal gas constant	R	8.31	J/mol·K
Model of Compliant Latex Valve			
Latex Thickness	N/A	0.000254	m
Hyperelastic Constant 1	s^+	1.5e-6	
Hyperelastic Constant 2	s^-	0.05e6	
Geometry of model (i.e. the gap between the latex and Nafion) are same as listed under generator geometry.			
Nitrogen Buildup Model			
Anode channel width	w_{ch}	0.8e-3	m
Anode channel height	h_{ch}	0.35e-3	m
Anode channel length	L_{ch}	0.1	m
Distance between anode channels	w_R	0.9e-3	m
Membrane thickness	δ	50e-6	m
First hydrogen permeability constant	$k_{H2,1}$	6.6e-11	$mol \cdot m^{-1} \cdot s^{-1} \cdot Pa^{-1}$
Second hydrogen permeability constant	$k_{H2,2}$	21.03e3	$J \cdot mol^{-1}$

First oxygen permeability constant	$k_{O2,1}$	0.5· $k_{H2,1}$	$mol \cdot m^{-1} \cdot s^{-1} \cdot Pa^{-1}$
Second oxygen permeability constant	$k_{O2,2}$	$k_{H2,2}$	$J \cdot mol^{-1}$
Hydrogen starvation mole fraction	$y_{H2,choking}$	0.01	N/A

APPENDIX

D

DIMENSIONS OF BENCHTOP FUEL CELL SYSTEM

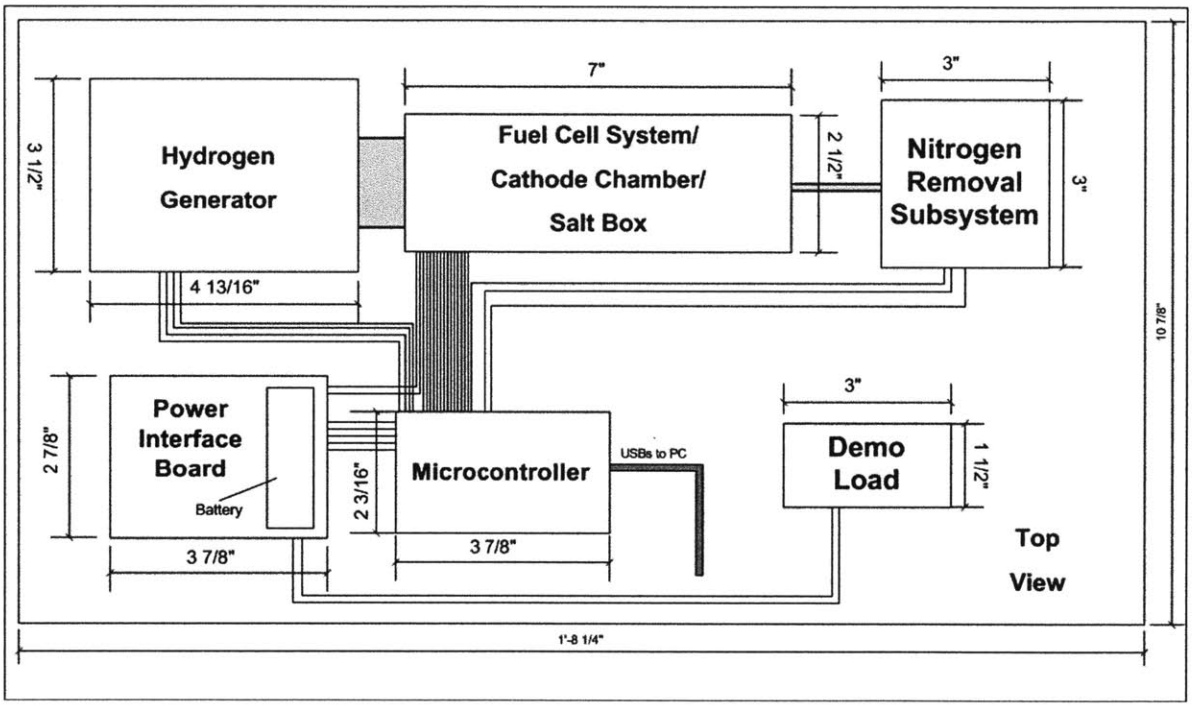

Figure 73: Dimensions of the benchtop fuel cell system.

Figure 73 shows a top view of the benchtop fuel cell system with dimensions. This is provided as a reference for the size of each of the subsystems.